Comput Mech (2012) 49:149–169
DOI 10.1007/s00466-011-0634-1

ORIGINAL PAPER

A new multiscale computational method for elasto-plastic analysis of heterogeneous materials

H. W. Zhang · J. K. Wu · J. Lv

Received: 14 December 2010 / Accepted: 13 July 2011 / Published online: 3 August 2011
© Springer-Verlag 2011

Abstract A new multiscale computational method is developed for the elasto-plastic analysis of heterogeneous continuum materials with both periodic and random microstructures. In the method, the multiscale base functions which can efficiently capture the small-scale features of elements are constructed numerically and employed to establish the relationship between the macroscopic and microscopic variables. Thus, the detailed microscopic stress fields within the elements can be obtained easily. For the construction of the numerical base functions, several different kinds of boundary conditions are introduced and their influences are investigated. In this context, a two-scale computational modeling with successive iteration scheme is proposed. The new method could be implemented conveniently and adopted to the general problems without scale separation and periodicity assumptions. Extensive numerical experiments are carried out and the results are compared with the direct FEM. It is shown that the method developed provides excellent precision of the nonlinear response for the heterogeneous materials. Moreover, the computational cost is reduced dramatically.

Keywords Multiscale computational method · Heterogeneous material · Base function · Elastoplasticity

H. W. Zhang (✉) · J. K. Wu · J. Lv
State Key Laboratory of Structural Analysis for Industrial Equipment, Department of Engineering Mechanics, Faculty of Vehicle Engineering and Mechanics, Dalian University of Technology, Dalian, 116024, People's Republic of China
e-mail: zhanghw@dlut.edu.cn

J. K. Wu
e-mail: jingkaiwu@mail.dlut.edu.cn

J. Lv
e-mail: lvjun@mail.dlut.edu.cn

1 Introduction

In the past few decades, composite materials are commonly used in industrial and engineering practice due to their excellent mechanical and physical properties, such as high strength and high stiffness, heat-resistance, low density, high damping, improved thermal conductivity, and so on. These materials always have multiple scale natures and are heterogeneous at a certain scale. The microstructure characteristics, including the sizes, morphologies, strengths and distributions of the heterogeneities, have a significant impact on the overall macroscopic behavior of composite materials. In order to optimize the composite materials and take advantage of the different properties of each component more reasonably, it is necessary to investigate the influence of the microstructures on the macroscopic performance. In principle the direct numerical methods by meshing all the heterogeneities can be applied for these problems, but such treatment will lead to systems with very large numbers of degrees of freedom when the materials are complicated and may be not practicable even using the advanced supercomputers, owing to the requisite of a tremendous amount of computer memory and CPU time. Thus, it has become an essential problem to develop effective computing models of heterogeneous materials in the practice engineering.

A large body of research has been performed to obtain the effective material properties of heterogeneous media through various multiscale modeling techniques. Kanoute et al. [1] reviewed some commonly used multiscale methods in the context of modeling mechanical and thermomechanical responses of composites. Among them, macroscopic effective constitutive response is predicted as a result of the analytical or numerical solution of a boundary value problem at the microscopic level. For the analytical approach, Eshelby [2] considered the shape of the inhomogeneity by

means of the Eshelby tensor and proposed the equivalent inclusion method. The method was further developed by a number of authors, for example, Hashin and Strikman [3], Mori and Tanaka [4], Hill [5], Christensen and Lo [6], Hori and Nemat-Nasser [7], et al. Also, there are some other analytical methods, such as the transformation field analysis theory [8]. However, there are a few restrictions when these simplified micromechanics models are used to solve the nonlinear problems, since they are difficult in capturing accurately the detailed microscopic stress and strain information in the complicated structures.

To overcome these difficulties, some numerical multiscale methods for heterogeneous materials are proposed and become increasing popular. In general, two different kinds of these numerical approaches can be distinguished. The first one concerns the case where the scales of microscopic and macroscopic can be fully separated. Notable among this kind of approaches is the asymptotic computational homogenization method, also called global-local analysis, which was first proposed by Benssousan and Lions [9] and Suquet [10] et al. In this method, the FEM is applied to obtain the homogenized material parameters as well as evaluate the valuable information on the local micro-scale fields from the macroscopic responses [11]. The computational homogenization method has been extensively studied and extended for solving various kinds of nonlinear problems, such as, small deformation elasto-plastic problems [12–18], local damage problems [19,20] and dynamic wave propagation problems [21–23]. Despite its overall success, the asymptotic computational homogenization method also has some limitations. For example, the numerical procedure is constructed by assuming the local periodicity on the RVEs. However, in practice, many heterogeneous materials have more or less arbitrariness in the size and distribution of constituents. In order to adapt to general heterogeneous materials, the size of RVE must be sufficiently large to contain enough microscopic heterogeneous information [13], which results in increase of the computational cost.

The second kind of approaches concerns the case where the characteristic length of microscale is not small enough to satisfy the assumption of the scale separation (e.g. see [24–26] and the references therein). This kind of approach requires that special strategies are needed for bridging the micro- and macro-scale directly. In present paper, we treat the problems of this kind. For this purpose, we inherit the basic idea of the multiscale finite element method (MsFEM), which can be traced back to the work presented by Babuska et al. [27,28] and was further developed by Hou et al. [29,30] for solving second-order elliptic boundary value problems with high oscillating coefficients. The MsFEM provides an effective way to capture the large-scale solutions on a coarse-scale mesh without resolving all the small-scale features. This is accomplished by constructing the multiscale base functions (shape functions) that are adaptive to the local property of the differential operator. The method has been successfully used for the numerical simulation of the two-phase flow and transport in highly heterogeneous porous media [31–34] and extended to solve the nonlinear partial differential equations [35]. Moreover, several similar multiscale methods have been developed, such as the multiscale finite volume method [36] and the finite volume multiscale finite element method [37]. However, fewer works discuss about the applications of the MsFEM for the vector field problems in the computational solid mechanics. It seems that the method will face some difficulties when it is extended to deal with the problems in solid mechanics where the bulk expansion/contraction phenomena (i.e., Poisson's effect) have to be considered in the construction of the base functions.

In order to solve the problems in solid mechanics, an extended mutilscale finite element method (EMsFEM), in which the additional coupling terms of the numerical base functions for the interpolation of the displacement field are introduced to consider the coupling effect among different directions in multi-dimensional vector problems, was proposed by Zhang and his coworkers [38]. By doing this, the microscopic heterogeneous features of elements can be well captured by the numerical base functions in the solid deformation. The EMsFEM has been successfully used for the elastic [38] and elasto-plastic [39] analyses of the periodic lattice truss materials. The above-mentioned researches show that, the downscaling computation in the EMsFEM can be implemented easily and the detailed microscopic stress and strain fields can be obtained simultaneously as well as the macroscopic responses. Thus, the EMsFEM has great potential for nonlinear analysis of heterogeneous materials.

In this paper, the EMsFEM is further developed for modeling the elasto-plastic behavior of heterogeneous continuum materials. The small deformation of elasto-plastic materials with the von Mises yield criterion is assumed. Both the materials with periodic and random microstructures are considered. A large number of numerical experiments have shown that the boundary conditions for the construction of the base functions play a key role on the accuracy of the multiscale method. A good choice of the boundary conditions can significantly improve the numerical precision. Thus, two new kinds of boundary conditions, i.e., the periodic boundary conditions and generalized periodic boundary conditions are introduced for the construction of the numerical base functions. They are expected to reflect better the nature of the underlying heterogeneities of coarse elements. With the evolution of microscopic stress in the nonlinear analysis, the unbalanced nodal forces in micro-scale are treated as the combined effects of macroscopic equivalent forces and microscopic perturbed forces by a special technique under the condition of consistency, in which the macroscopic equivalent forces are used to solve the macroscopic displacement field and microscopic perturbed forces are used to obtain the detailed stress

and strain in the micro-scale. Then the two-scale computational strategy with successive iteration scheme is proposed in the framework of nonlinear analysis. Extensive numerical examples are carried out and the results are compared with the traditional FEM which is applied directly on the resolved fine grids. The results show that the EMsFEM developed provides excellent precision of the nonlinear response for the heterogeneous materials, especially under the (generalized) periodic boundary conditions. Meanwhile, we will show that, the computer memory and CPU time required in our method are reduced dramatically.

Note that, unlike classical homogenization based approaches, since a full representation of the microstructure is solved directly on each coarse element rather than at the Gauss points of element, the method can obtain more accuracy results about the real microscopic stress and strain information. This is quite advantageous for strength and nonlinear analyses of heterogeneous materials, particularly when the stress and strain values in each element on micro scale are required. Moreover, the scale separation and periodicity assumption are no longer required in the current research, which further widen the range of applications of the method.

This paper is organized as follows. In the next section, the base equations for the elasto-plastic problems of continuum materials are briefly given. In Sect. 3, we present in detail the construction process of the numerical base functions for the displacement field of a coarse element, in which different kinds of boundary conditions for the construction of the base functions are presented. In Sect. 4, the equivalent stiffness matrix of a coarse element is deduced. Then, the downscaling computation technique of the EMsFEM is presented in Sect. 5, by which the real microscopic variables within the elements can be obtained easily. In Sect. 6, after introducing the equivalent technique of microscopic nodal forces (unbalanced forces) in the EMsFEM, the two-scale computational modeling with successive iteration scheme is proposed in the context of nonlinear analysis. Also, the flow charts of the implementation processes are provided. In Sect. 7, several illustrative numerical examples are conducted and the results are compared with the direct FE method to examine the validity of the EMsFEM. Then, the computer memory and CPU time are compared between the two methods to show the efficiency of the new method in Sect. 8. Finally, some discussions are presented.

2 Basic equations of the elasto-plastic problems

In this section, we briefly present the basic equations for the small deformation elasto-plastic analysis of continuum materials. Also, some notations and assumptions that will be used in the subsequent sections are provided.

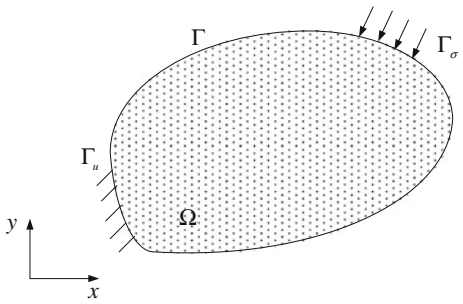

Fig. 1 Illustration of the heterogeneous body

Consider an elasto-plastic continuum body occupying a region Ω and having a boundary Γ depicted in Fig. 1. The boundary is constrained in some regions, where displacements are specified. Also, on part of the boundaries, distributed force per length, called traction, is applied. Note that only the plane strain problems are considered in this paper. The equilibrium equation and boundary conditions can be expressed as

$$\begin{aligned} &div\,(\mathbf{D}:\boldsymbol{\varepsilon}(\mathbf{u})) = \bar{\mathbf{f}} && \text{in } \Omega \\ &\mathbf{n}\boldsymbol{\sigma} = \overline{\mathbf{T}} && \text{on } \Gamma_\sigma \\ &\mathbf{u} = \bar{\mathbf{u}} && \text{on } \Gamma_u \end{aligned} \tag{1}$$

where $\mathbf{D}$ is the fourth-order stiffness tensor representing material properties, $\boldsymbol{\varepsilon}(\mathbf{u})$ is the strain tensor given as

$$\boldsymbol{\varepsilon}(\mathbf{u}) = \frac{1}{2}\left(\nabla\mathbf{u} + (\nabla\mathbf{u})^T\right) \tag{2}$$

and $\mathbf{u}$ is the displacement vector; $\boldsymbol{\sigma}$ is the stress tensor which has four independent components, $\boldsymbol{\sigma} = \left[\sigma_x\ \sigma_y\ \sigma_z\ \tau_{xy}\right]^T$; $\bar{\mathbf{f}}$ is the body force vector, $\bar{\mathbf{f}} = \left[\overline{f}_x\ \overline{f}_y\right]^T$; Γ_σ and Γ_u are the force and displacement boundary conditions, respectively; $\mathbf{n}$ is the unit normal matrix given as

$$\mathbf{n} = \begin{bmatrix} n_x & 0 & 0 & n_y \\ 0 & n_y & 0 & n_x \end{bmatrix} \tag{3}$$

The strain increment is decomposed into the elastic and plastic parts, $d\boldsymbol{\varepsilon}^e$ and $d\boldsymbol{\varepsilon}^p$, such that

$$d\boldsymbol{\varepsilon} = d\boldsymbol{\varepsilon}^e + d\boldsymbol{\varepsilon}^p \tag{4}$$

Also, we have the following constitutive relations

$$d\boldsymbol{\sigma} = \mathbf{D}^e(d\boldsymbol{\varepsilon} - d\boldsymbol{\varepsilon}^p) \tag{5}$$

where $\mathbf{D}^e$ is the fourth-order elasticity tensor.

For simplicity, we assume that the elasto-plastic materials defined here obey the Mises yield criterion with linear isotropic hardening. For the classical rate-independent J_2 elasto-plasticity, the yield function, plastic flow rule, loading/unloading condition of the Karush–Kuhn–Tucker form and the plastic consistency condition are given as,

respectively

$$f(\boldsymbol{\sigma}, \boldsymbol{\xi}) = \bar{\sigma} - \sigma_Y(\bar{\varepsilon}^p) \tag{6}$$

$$d\boldsymbol{\varepsilon}^p = d\lambda \frac{\partial Q}{\partial \boldsymbol{\sigma}} \tag{7}$$

$$f \le 0, \quad \lambda \ge 0, \quad f\lambda = 0 \tag{8}$$

$$\dot{f} = 0 \tag{9}$$

where $\bar{\sigma}$ and σ_Y are the equivalent stress and yield stress, respectively, which can be expressed as

$$\bar{\sigma} = \sqrt{\frac{3}{2}\boldsymbol{\sigma}^{\mathrm{dev}}:\boldsymbol{\sigma}^{\mathrm{dev}}}, \sigma_Y = \sigma_Y^0 + H\bar{\varepsilon}^p \tag{10}$$

where $\boldsymbol{\sigma}^{\mathrm{dev}} = \boldsymbol{\sigma} - (1/3)tr(\boldsymbol{\sigma})\mathbf{I}$ denotes the deviatoric stress tensor and $\mathbf{I}$ is the second-order symmetric unit tensor, σ_Y^0 is the initial yield stress, H is the hardening modulus, $\lambda \ge 0$ is the plastic multiplier, $\boldsymbol{\xi}$ is the vector of internal state variable for the strain hardening and can be identified with the equivalent plastic strain such that

$$\boldsymbol{\xi} := \bar{\varepsilon}^p = \int \sqrt{\frac{2}{3}} \left| d\boldsymbol{\varepsilon}^p \right| = \int \left(\frac{2}{3} d\varepsilon_{ij}^p d\varepsilon_{ij}^p \right)^{1/2} \tag{11}$$

In the case of associative plasticity, the flow potential function Q is the same as f, so the associative flow rule of plastic deformation can be given as follows

$$d\boldsymbol{\varepsilon}^p = d\lambda \frac{\partial f}{\partial \boldsymbol{\sigma}} = d\lambda \frac{3}{2} \frac{\boldsymbol{\sigma}^{\mathrm{dev}}}{\bar{\sigma}} \tag{12}$$

The above descriptions are referred to as the fine-scale model problems. For the problems with multiscale feature, the length scale of heterogeneities ε is much smaller than the macroscopic scale of structures. A meaningful solution is obtained with traditional FEM only if the finite element's mesh size h is smaller than the finest scale, i.e., $h \ll \varepsilon$, which is prohibitive due to that it requires a tremendous amount of computing resource. While for the EMsFEM developed in the following sections, since the small scale information can be effectively captured on the large-scale through the numerical multiscale base functions, then the problems can be solved using a mesh of size $h \gg \varepsilon$, thus resulting in a reduced number of degrees of freedom in the computational model.

3 The construction of numerical base functions

Let us consider the fine and coarse discretization meshes as shown in Fig. 2. For the EMsFEM, the main work is to numerically construct the multiscale base functions of each coarse-grid element. Then the small scale information is gathered into large scale through the equivalent stiffness matrices. By this way, the effect of small scale is well captured on the large scales.

For the vector field problems of computational solid mechanics, Numerical experiments have shown that the multiscale base functions used for the displacement interpolation in different coordinate directions are no longer the same for the coarse-grid elements with heterogeneous media. Thus the multiscale base functions for the displacement field should be constructed separately for different direction components. In the two-dimensional problems, two forms of base functions are constructed, in which one is used for the displacement interpolation in the x-direction and the other is used for the y-direction. In addition, to consider the coupling effect among different directions in the solid deformation, the additional coupling terms of the displacement fields are introduced into the multiscale base functions. The multiscale element then becomes mixed-interpolation type.

Take one of the coarse elements shown in Fig. 2 for example, the element occupying a region $\mathbf{K}, \mathbf{K} \subset \Omega$. The base functions are constructed by solving the equilibrium equation in region $\mathbf{K}$ with some specified boundary conditions.

From Eqs. 1 and 2, the general expression for solving the base functions of a two-dimensional problem can be given

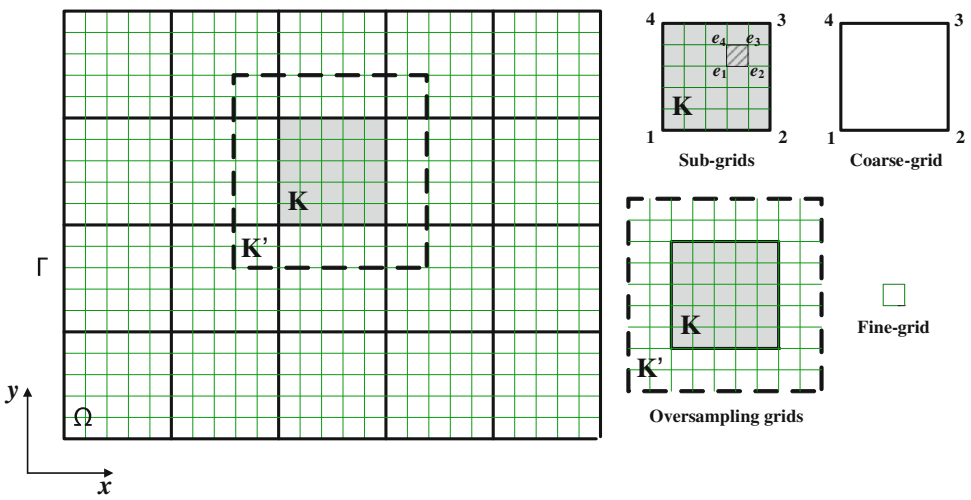

Fig. 2 Schematic description of the EMsFEM

as follows

$$\begin{array}{ll} \mathbf{L}\mathbf{N}_i = 0 & \text{in } \mathbf{K} \\ \mathbf{N}_i(\mathbf{x},\mathbf{y}) & \text{affined on } \partial\mathbf{K} \\ i = 1, 2, \ldots, m & \end{array} \tag{13}$$

where $\mathbf{L}$ is the calculation operator and satisfies $\mathbf{Lu} = div\left(\mathbf{D} : \frac{1}{2}\left(\nabla\mathbf{u} + (\nabla\mathbf{u})^T\right)\right)$; m means the node number of a coarse element and $m = 4$ is used in the current research.

Equation 13 is solved with the following boundary condition

$$\mathbf{N}_i = \mathbf{N}_i^0 \quad \text{on } \partial\mathbf{K} \tag{14}$$

where $\mathbf{N}_i$ is the base function of a coarse-grid node i and has two forms, i.e., $\mathbf{N}_i^x$ and $\mathbf{N}_i^y$. It satisfies $\mathbf{N}_i|_j = \delta_{ij}$, $(i, j = 1, 2, \ldots, m)$, where $\mathbf{N}_i|_j = \mathbf{N}_i(x_j, y_j)$ is defined and δ is the Kronecker delta; $\mathbf{N}_i^0$ is the boundary value imposed for the construction of the base function $\mathbf{N}_i$. In general, Eqs. 13 and 14 are solved with the traditional FEM on the corresponding fine-scale grids (i.e., sub-grids shown in Fig. 2) to compute the base functions $\mathbf{N}_i$.

Once the base functions have been constructed, the displacement fields within a coarse element can be expressed as

$$u = \sum_{i=1}^{4} N_{ixx} u_i' + \sum_{i=1}^{4} N_{ixy} v_i' \tag{15}$$

$$v = \sum_{i=1}^{4} N_{iyy} v_i' + \sum_{i=1}^{4} N_{iyx} u_i' \tag{16}$$

in which N_{iyx}(or N_{ixy}) is introduced which is an additional coupling term and means the displacement field in the y-direction (or x-direction) within the element induced by unit displacement of node i in the x-direction (or y-direction).

The base functions constructed should satisfy

$$\begin{cases} \sum\limits_{i=1}^{4} N_{ixx} = 1, & \sum\limits_{i=1}^{4} N_{iyy} = 1 \\ \sum\limits_{i=1}^{4} N_{iyx} = 0, & \sum\limits_{i=1}^{4} N_{ixy} = 0 \end{cases} \tag{17}$$

Equations 15 and 16 can be expressed in a unified form

$$\mathbf{u} = \mathbf{N}\mathbf{u}_\mathbf{E}' \tag{18}$$

where $\mathbf{N}$ is the base function matrix of a coarse grid element, $\mathbf{u}$ is the displacement vector of the nodes in the fine-scale mesh, and $\mathbf{u}_\mathbf{E}'$ is the displacement vector of nodes in the macro level. They can be expressed as

$$\begin{aligned} \mathbf{u} &= [u_1\ v_1\ u_2\ v_2\ \cdots\ \cdots\ u_n\ v_n]^T \\ \mathbf{N} &= \left[\mathbf{R}_1^T\ \mathbf{R}_2^T\ \cdots\ \mathbf{R}_n^T\right]^T \\ \mathbf{u}'_\mathbf{E} &= \left[u_1'\ v_1'\ u_2'\ v_2'\ u_3'\ v_3'\ u_4'\ v_4'\right]^T \end{aligned} \tag{19}$$

where

$$\mathbf{R}_i = \begin{bmatrix} N_{1xx}(i) & N_{1xy}(i) & N_{2xx}(i) & N_{2xy}(i) & N_{3xx}(i) & N_{3xy}(i) & N_{4xx}(i) & N_{4xy}(i) \\ N_{1yx}(i) & N_{1yy}(i) & N_{2yx}(i) & N_{2yy}(i) & N_{3yx}(i) & N_{3yy}(i) & N_{4yx}(i) & N_{4yy}(i) \end{bmatrix} \quad i = 1, 2, \ldots\ldots, n \tag{20}$$

and n is the total node number of the fine-scale mesh within the sub-grids.

As mentioned by many researchers [29–32,38,39], the choice of the boundary conditions $\mathbf{N}_i^0$ for the construction of the base functions has a big influence on the accuracy of the multiscale solutions. References [38,39] have proposed two kinds of boundary conditions, i.e., linear boundary conditions and oscillatory boundary conditions with oversampling technique, for the construction of the base functions. In this paper, two new kinds of boundary conditions (i.e., periodic boundary conditions and generalized periodic boundary conditions) are introduced. In the following, we take the construction of $\mathbf{N}_1^x = \{N_{1xx}, N_{1yx}\}$ as an example to show the basic construction process of the numerical base functions.

3.1 Linear boundary conditions (EMsFEM-L)

As shown in Fig. 3, for the linear boundary conditions, a unit displacement is applied on the node 1 in the x-positive direction, and the values vary linearly along boundaries 12 and 14, just as in the standard bilinear (linear) base functions, while the displacements on boundaries 34 and 23 are constrained in the x-direction to avoid rigid displacement. At the same time, the displacements of the boundary nodes of the sub-grids are all constrained in the y-direction. Using the boundary conditions mentioned above, the internal displacement field of the coarse element can be obtained by solving the equilibrium equation (Eq. 13) on the sub-grids with the standard finite element analysis. Therefore, the numerical base function $\mathbf{N}_1^x$ is obtained. The rest of base functions of the coarse element can be constructed in a similar way.

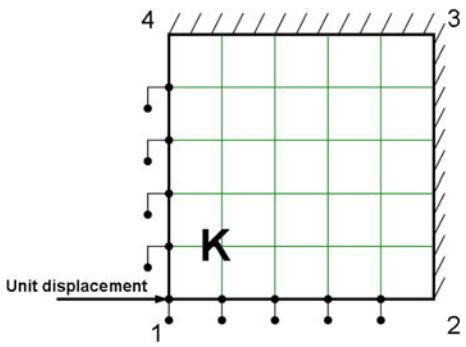

Fig. 3 The construction of base functions $\mathbf{N}_1^x$

3.2 Oscillatory boundary conditions with oversampling technique (EMsFEM-O)

It is easy to know that the linear boundary conditions impose too strong restrictions on the deformation of the boundary layer of the coarse elements. These artificial constraints will make the equivalent stiffness matrices of elements overestimate, especially for highly heterogeneous materials. The oversampling technique will relieve this difficulty in some degrees. Note that unlike the scalar problems [29–31], the oversampling technique is used here just for obtaining the oscillatory boundary conditions, which are further applied for the construction of base functions of the target coarse elements.

Consider a larger domain $\mathbf{K}'$ that covers the coarse element as illustrated in Figs. 2 and 4, in which $\Delta 1234$ is the original element (target coarse element) and $\Delta 1'2'3'4'$ is the oversampling element. Firstly, the temporary base functions $\boldsymbol{\psi}_{j'}(j' = 1', 2', 3', 4')$ of the oversampling element are constructed with the linear boundary conditions shown in Fig. 4 (here, $\psi_{1'xx}$ is taken as an example), without consideration of the additional coupling terms in the base functions. Then the temporary base functions $\boldsymbol{\varphi}_i$ of the original element are constructed through the linear combination of $\boldsymbol{\psi}_{j'}$, i.e.

$$\phi_{ixx} = \sum_{j=1}^{4} c_{ij}^{x} \psi_{j'xx} \tag{21a}$$

$$\phi_{iyy} = \sum_{j=1}^{4} c_{ij}^{y} \psi_{j'yy} \tag{21b}$$

where c_{ij}^{x} and c_{ij}^{y} are the constants determined by the conditions $\phi_{ixx}|_j = \delta_{ij}$ and $\phi_{iyy}\big|_j = \delta_{ij}$, respectively. The temporary base functions $\boldsymbol{\varphi}_i$ obtained satisfy $\sum_{i=1}^{4} \phi_{ixx} = 1$, $\sum_{i=1}^{4} \phi_{iyy} = 1$. Then, the boundary node values of $\boldsymbol{\varphi}_i$ are extracted and used as the oscillatory boundary conditions for constructing the final base functions. Without loss of generality, $\mathbf{N}_i^x = \{N_{ixx}, N_{iyx}\}$ can be obtained by solving the following problem

$$\begin{aligned} &\mathbf{L}\mathbf{N}_i^x = 0 && && \text{in } \mathbf{K} \\ &N_{ixx}(\mathbf{x}) = \phi_{ixx}, && N_{iyx}(\mathbf{x}) = 0 && \text{on } \partial\mathbf{K} \\ &i = 1, 2, ..., m \end{aligned} \tag{22}$$

The final base functions, i.e., N_{ixx}, N_{ixy}, N_{iyy} and N_{iyx}(i = 1,2,3,4) obtained by this way also satisfy Eq. 17.

3.3 Periodic boundary conditions (EMsFEM-P)

For the materials with periodic microstructures, we consider a RVE (unit cell), with vertices 1, 2, 3, 4 that are interconnected by boundaries Γ_{12}, Γ_{23}, Γ_{43} and Γ_{14}, as shown in Fig. 5. Instead of the prescribed displacements which are common in the linear boundary conditions, kinematical constraints are applied to the boundaries to ensure periodicity of the model in the deformed configuration. Take the construction of $\mathbf{N}_1^x$ for example, as illustrated in Fig. 5, the boundary conditions for a pair of the corresponding nodes $(\mathrm{A}^+,\mathrm{A}^-)$ on opposite edges Γ_{12} and Γ_{43}, can be given as

$$\begin{cases} u^{\mathrm{A}^+} - u^{\mathrm{A}-} = \Delta x \\ v^{\mathrm{A}^+} = v^{\mathrm{A}^-} \end{cases} \tag{23}$$

Similarly, for a pair of the corresponding nodes (B^+, B^-) on the opposite edges Γ_{14} and Γ_{23}, the boundary conditions can be expressed as

$$\begin{cases} u^{\mathrm{B}^+} - u^{\mathrm{B}-} = \Delta y \\ v^{\mathrm{B}^+} = v^{\mathrm{B}^-} \end{cases} \tag{24}$$

where, Δx and Δy are the given constants, whose values at node 1 are both set to be 1, and are both set to be 0 at nodes 2 and 4. For the other boundary nodes, the values of Δx and Δy vary linearly along edges Γ_{12} and Γ_{14}, respectively. The displacements of the node 3 are constrained in

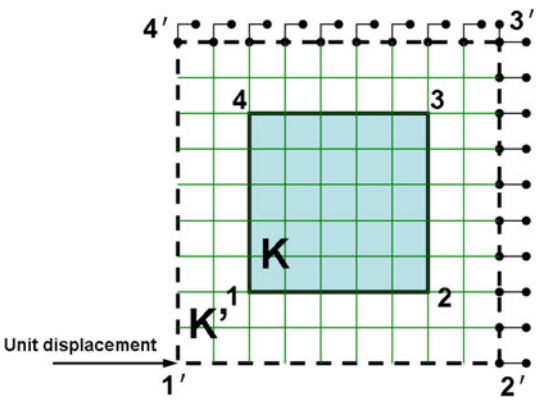

Fig. 4 Illustration of the oversampling technique

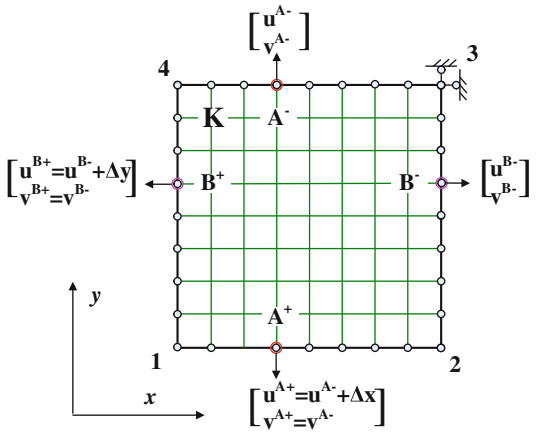

Fig. 5 Periodic boundary conditions for the construction of base function $\mathbf{N}_1^x$

both coordinate directions. Using the kinematical constraints described above, the whole displacement field of the coarse-grid element can be obtained by solving the equilibrium equation (Eq. 13) on the sub-grids with the standard finite element analysis. In this way, the numerical base functions can be obtained.

3.4 Periodic boundary conditions combined with the oversampling technique (generalized periodic boundary conditions) (EMsFEM-OP)

Combining the periodic boundary conditions and the oversampling technique mentioned above, the generalized periodic boundary conditions are introduced for random (non-periodic) heterogeneous materials. The main idea of this approach can be described as follows. First, the oversampling technique is only used to construct the oscillatory boundary conditions. Subsequently, based on the generated oscillatory boundary conditions, kinematical constraints are extracted and applied to the target grid element to compute the required multiscale base functions, which are different from the conventional oversampling technique where the generated oscillatory boundary conditions are directly imposed on the target coarse grid elements.

Take the construction of $\mathbf{N}_1^x$ for example, the numerical procedure requires three steps:

Step 1 The oversampling technique is utilized to obtain the oscillatory boundary conditions for the base functions, just the same as the step mentioned above for the oversampling technique. As an example illustrated in Fig. 5, the generated displacements in the x-direction of a pair of nodes $(\mathrm{A}^+,\mathrm{A}^-)$ on the opposite edges are u'_{A^+} and u'_{A^-}, respectively.

Step 2 With the oscillatory boundary conditions obtained above, the kinematical constraints are constructed and applied to the target coarse grid element, e.g., for the corresponding nodes $(\mathrm{A}^+,\mathrm{A}^-)$ (the kinematical constraints for the nodes $(\mathrm{B}^+,\mathrm{B}^-)$ can be constructed in the same way), the constraints can be written as

$$\begin{cases} u^{A^+} - u^{A^-} = u'_{A^+} - u'_{A^-} \\ v^{A^+} - v^{A^-} = 0 \end{cases} \tag{25}$$

Step 3 Using the kinematical constraints described above, the based functions can be constructed directly on the coarse grid element.

4 Equivalent stiffness matrix

Once the multiscale base functions are constructed, the equivalent stiffness matrix of a coarse element can be obtained under the conception of equivalence of strain energy, such that

$$\mathbf{K}_E = \sum_{e=1}^{p} \mathbf{K}'_e, \quad \mathbf{K}'_e = \mathbf{G}_e^T \mathbf{K}_e \mathbf{G}_e \tag{26}$$

where p is the total number of fine-scale elements within the sub-grids, $\mathbf{K}_e$ is the traditional stiffness matrix of a fine-scale element e (see Fig. 2), which can be expressed as

$$\mathbf{K}_e = \int_{\Omega_e} \mathbf{B}_e^T \mathbf{D}_e \mathbf{B}_e d\Omega_e \tag{27}$$

in which $\mathbf{B}_e$ and $\mathbf{D}_e$ are the strain-displacement matrix and material property matrix of the element e, respectively; $\mathbf{G}_e$ is a transition matrix which denotes the mapping relation between the displacement vectors of the micro-scale nodes and macro-scale nodes

$$\mathbf{u}_e = \mathbf{G}_e \mathbf{u}'_{\mathbf{E}}, \mathbf{G}_e = \begin{bmatrix} \mathbf{R}_{e1} \\ \mathbf{R}_{e2} \\ \mathbf{R}_{e3} \\ \mathbf{R}_{e4} \end{bmatrix} \tag{28}$$

where $\mathbf{u}_e$ is the displacement vector of element e.

In the same way, we can obtain all the equivalent element stiffness matrices of the coarse elements. Thus the equivalent global stiffness matrix of the overall structure is obtained as follows

$$\mathbf{K} = \mathop{\mathbf{A}}_{i=1}^{M} \mathbf{K}_{\mathbf{E}}^i \tag{29}$$

where $\mathbf{A}_{i=1}^{M}$ is a matrix assembled operator, and M is the total number of the coarse elements, $\mathbf{K}_E^i$ can be obtained from Eq. 26.

The traditional FEM is then, able to be carried out on the coarse-scale meshes, which reduces the degrees of freedom significantly in the macroscopic level computation. Thus, the macroscopic displacement vector $\mathbf{U}$ can be obtained by solving the following equation

$$\mathbf{KU} = \mathbf{F}_{ext} \tag{30}$$

where $\mathbf{F}_{ext}$ is a system of external forces subjected to the structure.

5 Downscaling computation

As for the EMsFEM, the relation between the micro- and macro- scales is created through the multiscale base functions which are constructed numerically and can reflect the micro-scale natures within each coarse element. Take advantage of this relation, the downscaling computation could be carried out easily and the detailed stress and strain information at the micro-scale can be obtained simultaneously in the multiscale computation as well as the macro displacement response of

the overall structure. Thus, the evolution of the microscopic variables accompany with the load steps can be well captured, which is important for the elasto-plastic analysis.

Take the fine-scale element e mentioned above as an example, the microscopic nodal displacements can be obtained through Eq. 28 when the macroscopic displacements have been obtained. Then, it is easy to obtain the strain and stress of element e by using the geometrical equation and the physical equation

$$\boldsymbol{\varepsilon}_e = \mathbf{B}_e\mathbf{u}_e = \mathbf{T}_e\mathbf{u}'_E, \quad \mathbf{T}_e = \mathbf{B}_e\mathbf{G}_e \tag{31}$$

and

$$\boldsymbol{\sigma}_e = \mathbf{D}_e\boldsymbol{\varepsilon}_e = \mathbf{S}_e\mathbf{u}'_E, \quad \mathbf{S}_e = \mathbf{D}_e\mathbf{B}_e\mathbf{G}_e \tag{32}$$

In practical implementation, the strain mapping matrix $\mathbf{T}_e$ and the stress mapping matrix $\mathbf{S}_e$ of the element e can be stored in a data base and do not need to be re-computed, then the microscopic strain and stress information can be conveniently obtained at each incremental step.

6 Two-scale modeling scheme for elasto-plastic analysis

In this section, a two-scale modeling scheme based on the EMsFEM for the elasto-plastic heterogeneous materials is developed and the flow charts of the algorithm are provided.

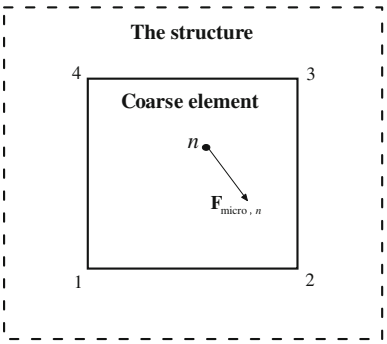

Fig. 6 A force applied on the node of microscale meshes of a coarse element which is contained in the structure

6.1 Treatment of micro-scale nodal forces

As we can see from Sect. 4 that, the problems are finally solved on the macro-scale once the equivalent stiffness matrices of coarse elements have been obtained. In this case, the external forces $\mathbf{F}_{ext}$ in the formula (30) should be applied on the macroscopic nodes. However, it is inevitable that some external forces are acted on the nodes of micro-scale meshes within the coarse elements. On the other hand, when material nonlinearity is considered in the multiscale analysis, it will induce unbalanced nodal forces in the micro-scale meshes with the emergence of plastic deformation. Thus, it is necessary to put forward an equivalent method to substitute the macroscopic nodal forces (i.e., the forces applied on the corner nodes of coarse elements) for the micro-scale nodal forces, and ensure that the global displacement response of structure and local micro-scale stress and strain response within the coarse elements are remain unchanged.

As shown in Fig 6, a force $F_{\text{micro,n}}$ is applied on the nth node of micro-scale meshes of a coarse element which is contained in the structure. In our method, the nodal forces in the micro-scale within the coarse element are treated as the combined effects of the macroscopic equivalent forces and microscopic perturbed forces (see Fig. 7a, b), in which the macroscopic equivalent forces (Fig. 7a) are used to solve the macroscopic displacement field and the microscopic perturbed forces (Fig. 7b) are used to obtain the local stress and strain in the micro-scale.

In reference [39] we have derived the macroscopic equivalent forces by virtue of the principle of virtual work, it can be expressed as

$$\mathbf{F}_{\mathbf{E},n} = \mathbf{F}_{\text{micro,n}}\mathbf{R}_n \tag{33}$$

in which $\mathbf{F}_{\mathbf{E},n} = \left[\mathbf{F}_{\mathbf{E1},n}\ \mathbf{F}_{\mathbf{E2},n}\ \mathbf{F}_{\mathbf{E3},n}\ \mathbf{F}_{\mathbf{E4},n}\right]$ are the macroscopic equivalent forces shown in Fig. 7a, and $\mathbf{F}_{\mathbf{E}i,n} = \left[F_{\mathbf{E}ix,n}\ F_{\mathbf{E}iy,n}\right]$ $(i = 1, 2, 3, 4)$. $\mathbf{R}_n$ is a part of the numerical base function that can be obtained by formula (20).

For the microscopic perturbed forces, since the periodic boundary conditions are used in this paper for the construction of numerical base functions, to be consistent, here we just

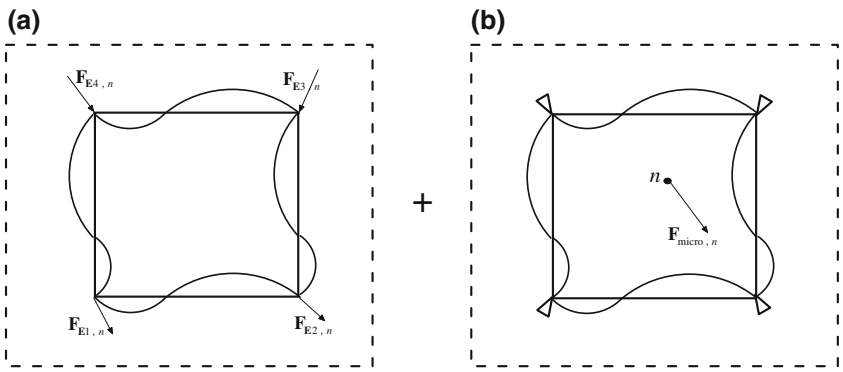

Fig. 7 Equivalence of micro-scale nodal force depicted in Fig 6: **a** macroscopic equivalent forces; **b** constrains for the microscopic perturbed forces

fix the four corner nodes of the coarse element in the x- and y-directions, while the other boundary nodes of the coarse element are constrained periodically as shown in Fig. 7b. Then the local effect of the microscopic perturbed force can be obtained by the conventional FE analysis on the sub-grids acted by the force $F_{\text{micro,n}}$ under the constraint conditions mentioned above.

6.2 Incremental iteration algorithm

In the numerical procedure of the EMsFEM, two-scale computational strategy is established to analyze the nonlinear problems, in which the macro-scale (coarse-scale) is used to solve the macroscopic displacement increment and the micro-scale (fine-scale) is adopted to obtain the evolution of the microscopic stress and strain. The link between the two scales is built through the numerical base functions.

As the analysis in Sect. 6.1, the temporary microscopic stress increment in the EMsFEM can be treated as combined effects of two items, that is

$$d\tilde{\boldsymbol{\sigma}} = d\sum + d\hat{\boldsymbol{\sigma}} \tag{34}$$

where $d\sum$ is the stress increment induced by the macroscopic displacement increment $\Delta\mathbf{U}$, and $d\hat{\boldsymbol{\sigma}}$ is the stress increment induced by the local effect of microscopic perturbed forces. Note that $d\hat{\boldsymbol{\sigma}}$ is set to zero vector for the first iteration step since no microscopic unbalanced forces exists.

To describe the evolution of plastic strains, we introduce a load parameter $t, 0 \le t \le T$. Now the load interval $[0, T]$ of interest is discretized into some nonoverlapping intervals $[0, T] = \cup_{n=0}^{N} [t_n, t_{n+1}]$. We assume that the solutions of variables $\boldsymbol{\varepsilon}_n^p, \boldsymbol{\sigma}_n, \boldsymbol{\xi}_n$ and $\mathbf{U}_n$ at load step t_n are given. Then the variables at t_{n+1} can be computed by using the following incremental FE algorithm in the interval $\Delta t = t_{n+1} - t_n$.

(a) For the macro-scale problems, we introduce the load increment parameter $\varsigma_{n+1} = (n+1)\Delta t/T$ and suppose that all the external forces $\mathbf{F}_{ext}$ are acted on the macroscopic nodes, thus we have

$$\Delta\mathbf{U} = \left[{}^{\tau}\mathbf{K}\right]^{-1} \Delta\mathbf{F}(t_n \le \tau \le t_{n+1}) \tag{35}$$

where

$$\Delta\mathbf{F} = (\varsigma_{n+1} - \varsigma_n)\,\mathbf{F}_{ext} \tag{36}$$

and

$${}^{\tau}\mathbf{K} = \mathop{\mathbf{A}}_{i=1}^{M} {}^{\tau}\mathbf{K}_E^i \tag{37}$$

where ${}^{\tau}\mathbf{K}_E^i$ is the equivalent stiffness matrix of the ith coarse element, M is the total number of coarse elements in the structure.

As we know that the equivalent stiffness matrix of the coarse element are derived by the numerical multiscale base functions whose values depend on the material properties of the fine-scale elements within the coarse element. For the material nonlinearity problems, the material property matrix $[\mathbf{D}]$ in Eq. 13 and $[\mathbf{D}_e]$ in Eq. 27 are changed along with the evolution of macroscopic displacements. That is to say, the Eq. 35 is a nonlinear system of equations. There are several common methods can be used for solving this problem, such as, the Newton-Raphson iteration (N-R) method, the modified Newton-Raphson iteration (mN-R) method and the initial stiffness iteration method. For the N-R method, it requires that the numerical base functions of coarse elements be re-constructed and the equivalent global stiffness matrix be re-formed and reduced in each iteration step. Whereas the mN-R method requires that the numerical base functions and the equivalent global stiffness matrix are updated only at the beginning of each increment step. It avoids the expensive repetitions of constructing base functions and forming equivalent matrix. However, more iterative steps are needed in order to reach the convergence. Generally speaking, the initial stiffness iteration method can be seemed as a special case of the mN-R method, whose base functions and equivalent stiffness matrix of each coarse element only need to be solved one time in the elastic stage and remain unchanged for the subsequent increment steps. For the sake of simplicity, in this paper, we just used the initial stiffness iteration method to solve the nonlinear system of equations.

It should be remarked that, though the initial stiffness iteration method refrains from recomputing the equivalent matrix thus overcomes a major computational cost, it sometimes will encounter convergence rate problem. Suppose elastic-perfectly plastic materials are used, the procedure may converge at a slow rate or even fail to converge. In such a case, the other iteration methods which have been developed for the high nonlinear analyses of elasto-plastic problems could be adopted.

(b) For the micro-scale problems, the unknown state variables at t_{n+1} can be computed in the following forms by virtue of the backward (implicit) Euler scheme [40]

$$\boldsymbol{\varepsilon}_{n+1} = \boldsymbol{\varepsilon}_n + \Delta\boldsymbol{\varepsilon} \tag{38}$$

$$\boldsymbol{\varepsilon}_{n+1}^p = \boldsymbol{\varepsilon}_n^p + \Delta\lambda_{n+1}\mathbf{r}_{n+1} \tag{39}$$

$$\boldsymbol{\xi}_{n+1} = \boldsymbol{\xi}_n + \Delta\boldsymbol{\xi} \tag{40}$$

$$\boldsymbol{\sigma}_{n+1} = \mathbf{D}^e{:}(\boldsymbol{\varepsilon}_{n+1} - \boldsymbol{\varepsilon}_{n+1}^p) \tag{41}$$

$$f_{n+1} = f(\boldsymbol{\sigma}_{n+1}, \boldsymbol{\xi}_{n+1}) = 0 \tag{42}$$

where $\mathbf{r} = \frac{\partial f}{\partial \boldsymbol{\sigma}}$ is the normal direction of the yield surface.

Using (12) and (41), the final updated stress $\boldsymbol{\sigma}_{n+1}$ can be expressed as follows

$$\boldsymbol{\sigma}_{n+1} = \boldsymbol{\sigma}^{\text{trial}} - \Delta\lambda\mathbf{D}^e{:}\frac{\partial f}{\partial \boldsymbol{\sigma}_{n+1}} \tag{43}$$

in which $\boldsymbol{\sigma}^{\text{trial}} = \boldsymbol{\sigma}_n + \mathbf{D}^e{:}\Delta\boldsymbol{\varepsilon}$ is the elastic trial stress. Here, the radial return algorithm [41] is applied to compute the returned stress.

6.3 Flow chart for the elasto-plastic multiscale computation

In the practical computation, there are two main implementation parts in the EMsFEM for elasto-plastic analysis:

1. *Preprocessing part* In this part, the numerical multiscale base functions of each coarse element are constructed, and the corresponding equivalent stiffness matrix of the coarse element is derived in the elastic situation. All these results are stored in the data base and can be obtained conveniently. Note that for the heterogeneous materials with periodic microstructures, the numerical base functions only need to be constructed one time on a unit cell. The flow chart for preprocessing part is plotted in Fig. 8.
2. *Iteration part* The nonlinear system is computed incrementally using the initial stiffness iteration scheme in the frame work of two-scale computational procedure. The algorithm is converged when macro- and micro-scale states are equilibrated simultaneously. We employ the following notation to denote the physical quantities in the iteration computation: $\bullet_n^{(j)}$, in which the right subscript n denotes the load increment and the right superscript (j) denotes the iteration count. Quantities without the right superscript, i.e., $\bullet_n$, denote the converged results at the load step n. Supposing that the values of variables $\boldsymbol{\sigma}_n$, $\boldsymbol{\varepsilon}_n^p$, $\boldsymbol{\xi}_n$ and $\mathbf{U}_n$ at the time load increment t_n are given. For the increment interval $\Delta t = t_{n+1} - t_n$, we have $\boldsymbol{\sigma}_{n+1}^{(0)} = \boldsymbol{\sigma}_n$, $\boldsymbol{\varepsilon}_{n+1}^{p(0)} = \boldsymbol{\varepsilon}_n^p$, $\boldsymbol{\xi}_{n+1}^{(0)} = \boldsymbol{\xi}_n$, $\mathbf{U}_{n+1}^{(0)} = \mathbf{U}_n$ and $\Delta\mathbf{F}_{n+1}^{(0)} = (\zeta_{n+1} - \zeta_n)\,\mathbf{F}_{ext}$. The flow chart of iteration part is plotted in Fig. 9.

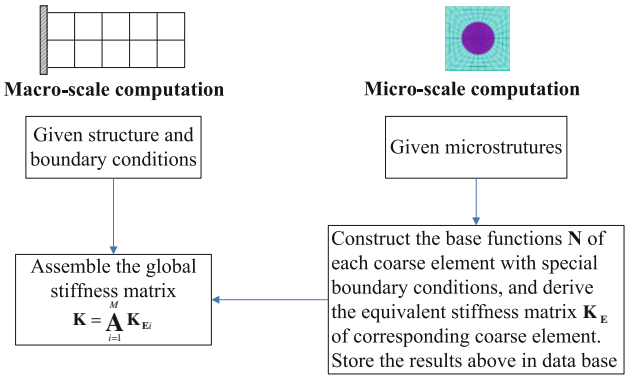

Fig. 8 Flow chart for the preprocessing part

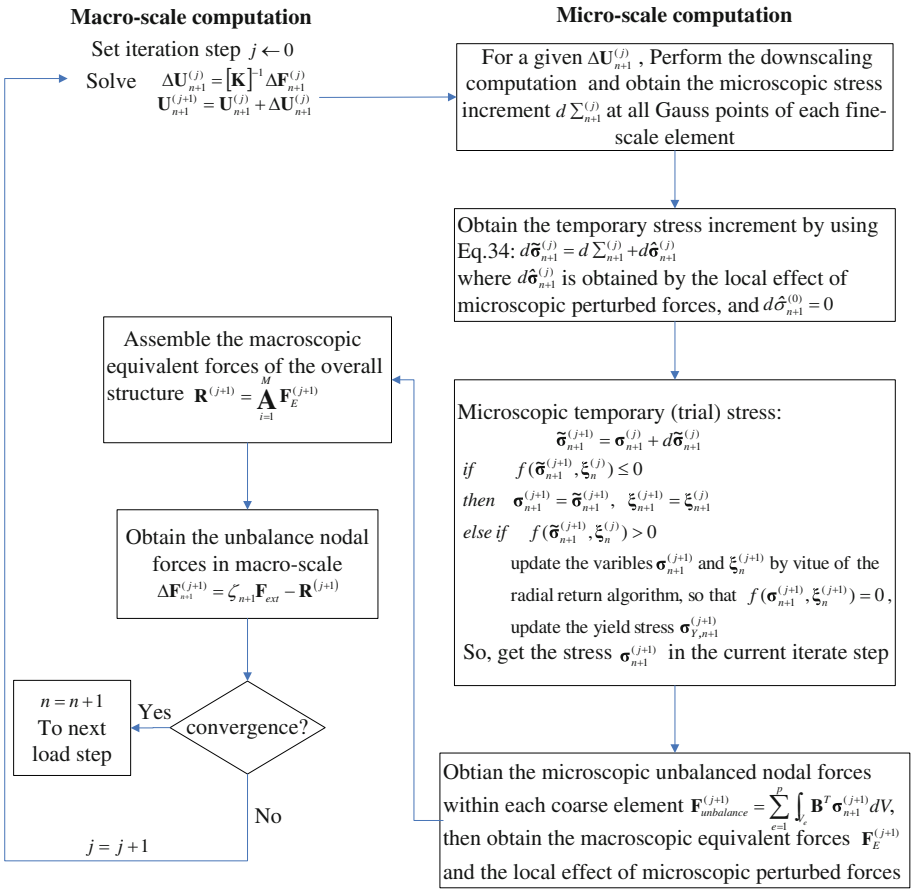

Fig. 9 Flow chart for the iteration part

7 Numerical examples

In this section, several representative numerical examples are presented for the analysis of elasto-plastic heterogeneous materials with both periodic and random microstructures. For the previous case, the linear and periodic boundary conditions are adopted for the constructions of multiscale base functions, respectively; while for the random one, the generalized periodic boundary conditions are used. To examine the validity of the developed method, the structures are also solved by the directed FEM on the fine-scale models (FEM-F), whose results can be seen as reference solutions. Note that plane strain is assumed here and all the parameters are dimensionless.

Example 1 For the first example, we consider a cantilever beam structure which is composed of 30×6 periodic microstructures. The macroscopic FE model is shown in Fig. 10, in which the x-displacement of the left edge of the structure and the y-displacement of the middle point on the left edge is fixed and a uniformly distributed load **F** is applied on right side with a magnitude of 1,000 and is divided into 10 steps. Three kinds of unit cells (see Fig. 11) are considered respectively in this example, in which the unit cell 1 is the two-phase composite material, the matrix (phase 1) behavior reveals the plastic deformation (obey the Mises yield criterion with linear isotropic hardening) with Young's modulus $E_e = 1.0e6$, Poisson's ratio $\mu = 0.3$, hardening modulus $H = 0.25e6$ and initial yield stress $\sigma_Y^0 = 700$, whereas the hard inclusion (phase 2) is assumed to never yields, with the following properties: $E_e = 1.0e7$ and $\mu = 0.3$; the unit cell 2 is porous material without phase 2; the unit cell 3 is solid and can be seen as homogeneous material.

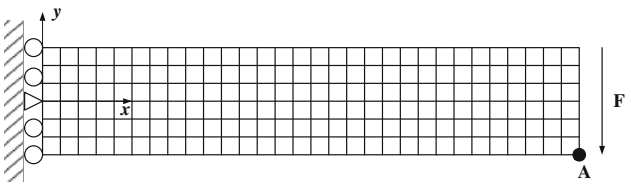

Fig. 10 Macroscopic FE model and its boundary conditions

Figures 12, 13 and 14 show the load-displacement curves at Point A obtained by the three methods for the structures with different unit cells. We can see that, for all cases the results obtained by the EMsFEM-P are more accuracy

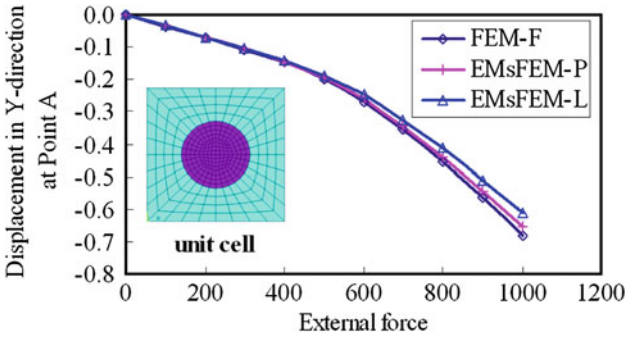

Fig. 12 Macroscopic load-displacement curves at Point A (unit cell 1)

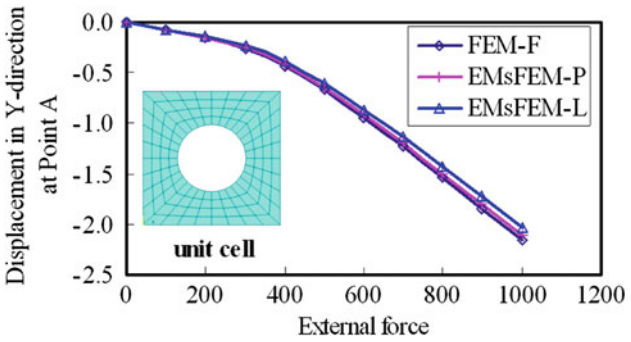

Fig. 13 Macroscopic load-displacement curves at Point A (unit cell 2)

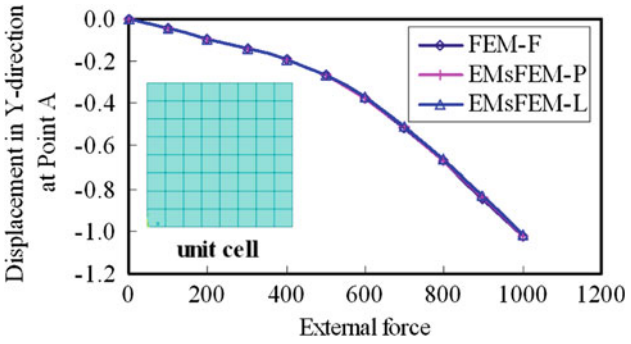

Fig. 14 Macroscopic load-displacement curves at Point A (unit cell 3)

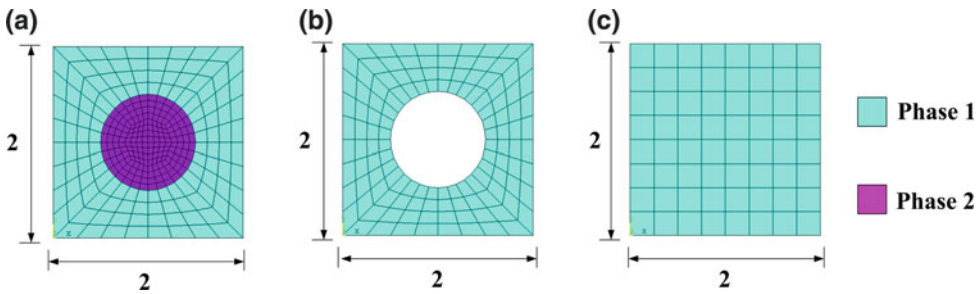

Fig. 11 Three kinds of microscopic FE models: **a** unit cell 1; **b** unit cell 2; **c** unit cell 3

than those obtained by the EMsFEM-L. It demonstrates that the periodic boundary conditions can simulate the deformation of unit cells within the structures more reasonably and improve convergence as opposed to linear boundary conditions. However, for the structures with the unit cell 1 and unit cell 2, there are also slight errors between the EMsFEM-P and the reference solutions. The maximum relative errors (i.e., at the final loading step) are 3.78 and 1.80% respectively for two different types of unit cell. The reasons of the errors of the EMsFEM-P are mainly arisen by the boundary effects of the structure in the frame work of two-scale procedure and will be discussed in the next numerical example in detail. For the structure with homogeneous unit cell (unit 3), both the EMsFEM-P and EMsFEM-L can yield almost the same results as the reference values. Figures 15, 16, 17, 18, 19 and 20 show the distributions of microscopic equivalent stress and equivalent plastic strain for the structures with different kinds of unit cells obtained by the FEM-F and EMsFEM-P. We can see that approving results can be obtained by the EMsFEM-P, whose results fit fairly well with those of the FEM-F. It illustrates that the EMsFEM-P can capture well the evolution of the microscopic variables.

Example 2 We explain the boundary effect of structure mentioned above through a simple, but illustrative numerical example. As shown in Fig. 21, the bottom of a plane strain structure is fixed in the y-direction and a uniformly distributed load $\mathbf{F}$=10,000 is applied on the top side. Also, the x-direction of the left lower corner of the structure is fixed to avoid the rigid body displacement. The structure is composed of 8×8 periodic unit cells. Only the unit cell 1 shown in Fig. 11a is considered here and the material properties are the same as Example 1 except that the initial yield stress for phase 1 here is $\sigma_Y^0 = 300$. The mesh discretization schemes for the EMsFEM and FEM-F are shown in Fig. 22a and b, respectively. Figure 23 shows the load-displacement curves at Point A obtained by the three methods. There are slight errors for the EMsFEM-P when the loading step increases, while for the EMsFEM-L, the results are obvious stiffer. The distributions of microscopic equivalent stress and equivalent plastic strain for the structure are shown in Figs. 24 and 25. We can see that,

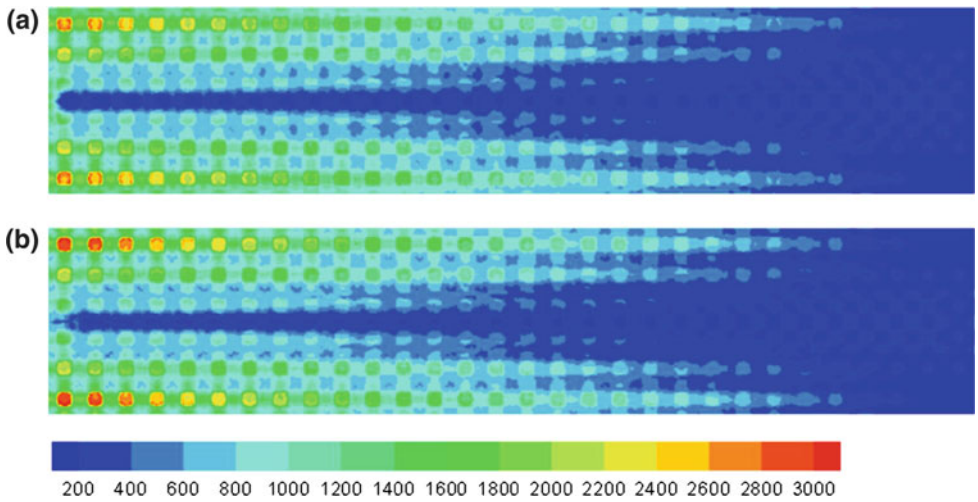

Fig. 15 Microscopic von-Mises stress at the final loading step (unit cell 1): **a** FEM-F; **b** EMsFEM-P

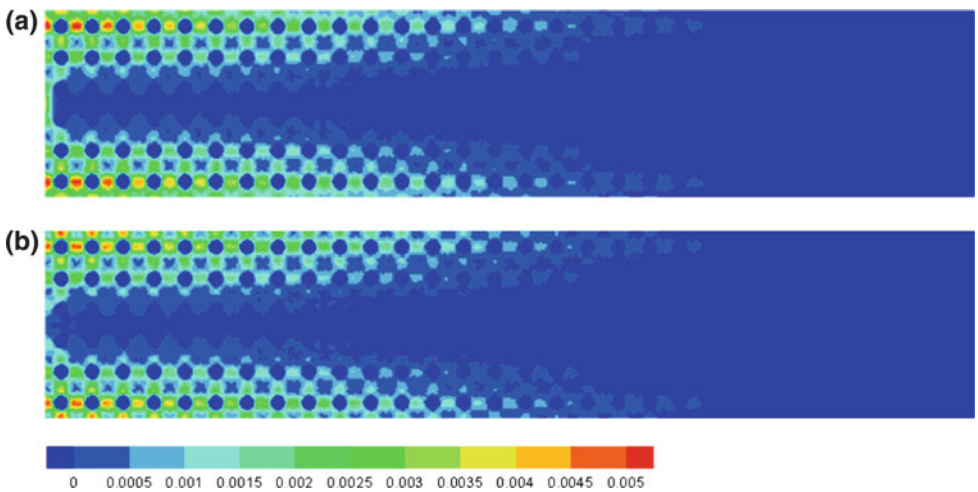

Fig. 16 Microscopic equivalent plastic strain at the final loading step (unit cell 1): **a** FEM-F; **b** EMsFEM-P

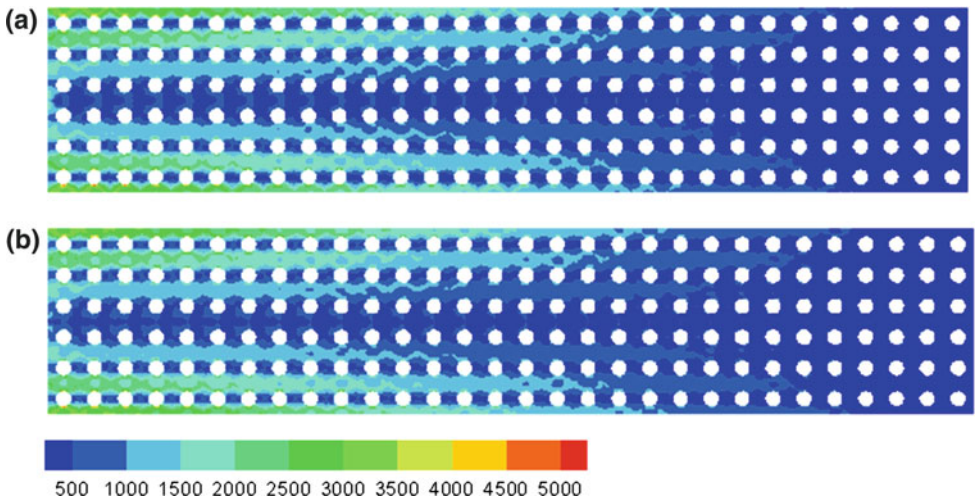

Fig. 17 Microscopic von-Mises stress at the final loading step (unit cell 2): **a** FEM-F; **b** EMsFEM-P

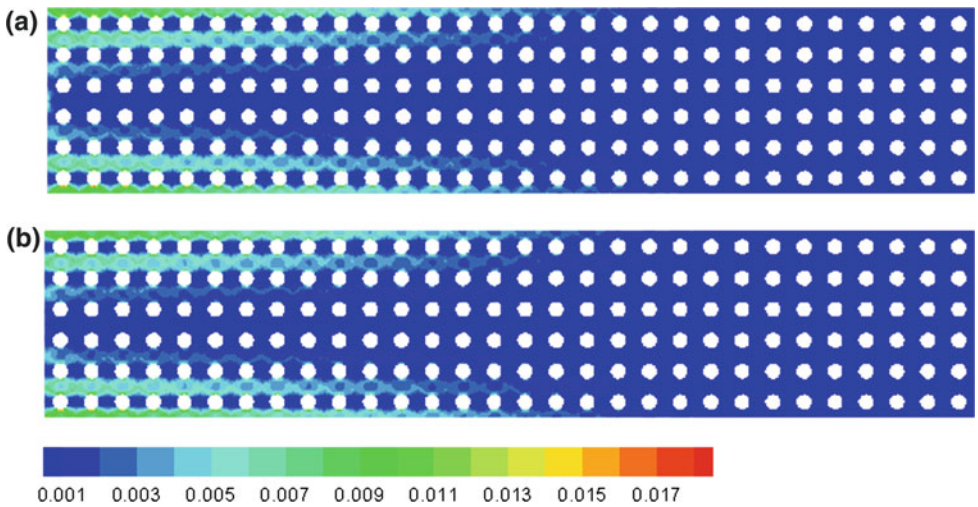

Fig. 18 Microscopic equivalent plastic strain at the final loading step (unit cell 2): **a** FEM-F; **b** EMsFEM-P

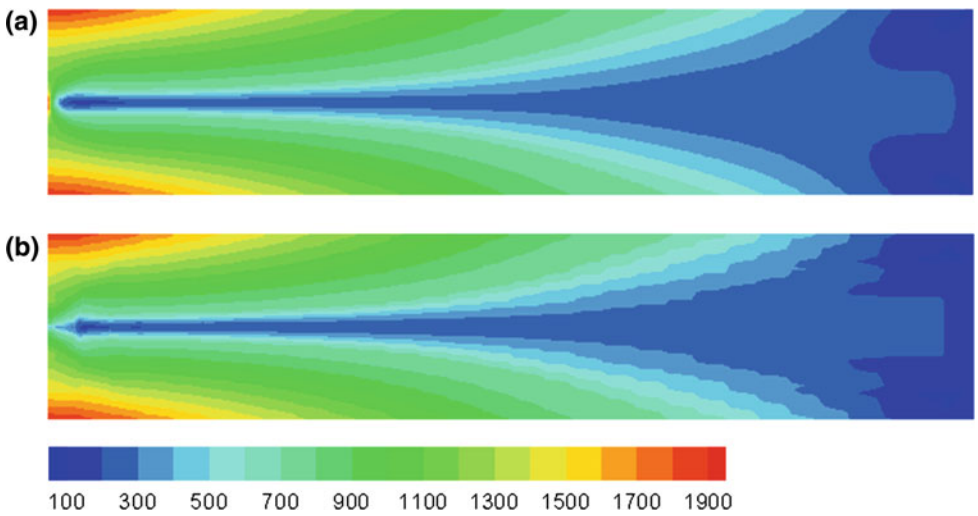

Fig. 19 Microscopic von-Mises stress at the final loading step (unit cell 3): **a** FEM-F; **b** EMsFEM-P

for the unit cells locate on the inside of the structure, both the distributions of microscopic equivalent stress and equivalent plastic strain obtained by the EMsFEM-P are almost the same with those of the FEM-F, while for the unit cells on the boundaries of the structure, the distributions obtained by the two methods have some differences. This is because that in the EMsFEM-P, the periodic boundary conditions are used for the construction of numerical base functions. In this

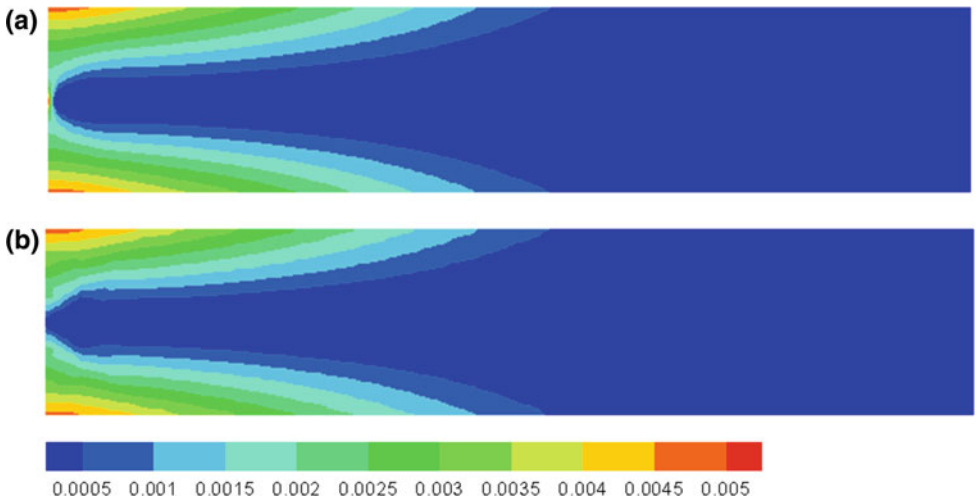

Fig. 20 Microscopic equivalent plastic strain at the final loading step (unit cell 3): **a** FEM-F; **b** EMsFEM-P

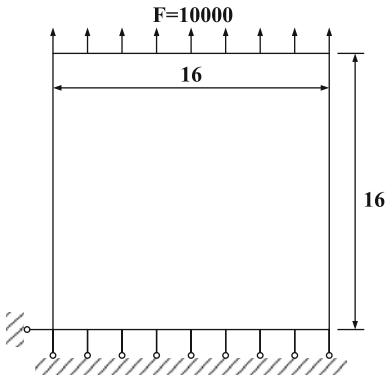

Fig. 21 Structure and its boundary conditions

context, the periodic deformations are happened for all the cells. While in practice, the fine-scale elements on the boundaries of structure are not constrained and can deformed freely. This to say, there are forcible deformations on the boundaries of the structure in the EMsFEM-P and lead to the errors, this problem also exists in other homogenization methods. However, we can see from the results in Figs. 12, 13, 14 and 23 that, the errors caused by the boundary effect of structure in the EMsFEM-P is very slight and the results meet the demand of precision. Moreover, when the number of unit cells contained in the structure increases (i.e., the proportion of the unit cells located on the boundaries of structure is reduced) or the unit cell tends to be homogeneous, the boundary effects will become more weaken. On the other hand, the results also illustrate that the periodic boundary conditions are more reasonable than linear boundary conditions and can reflect the nature of the underlying heterogeneities since the deformations of the inner unit cells fit very well with the direct FE solutions.

Example 3 Consider a macroscopic FE model shown in Fig. 26, which is composed of 16 × 10 periodic unit cells. The left and right sides of the model are fixed in the x-direction and the bottom of the model is fixed in the y-direction. A uniformly distributed load of 10,000 is applied on the top side and divided into 10 steps. The two-phase unit cell shown in Fig. 11a is also used in this example with the initial yield

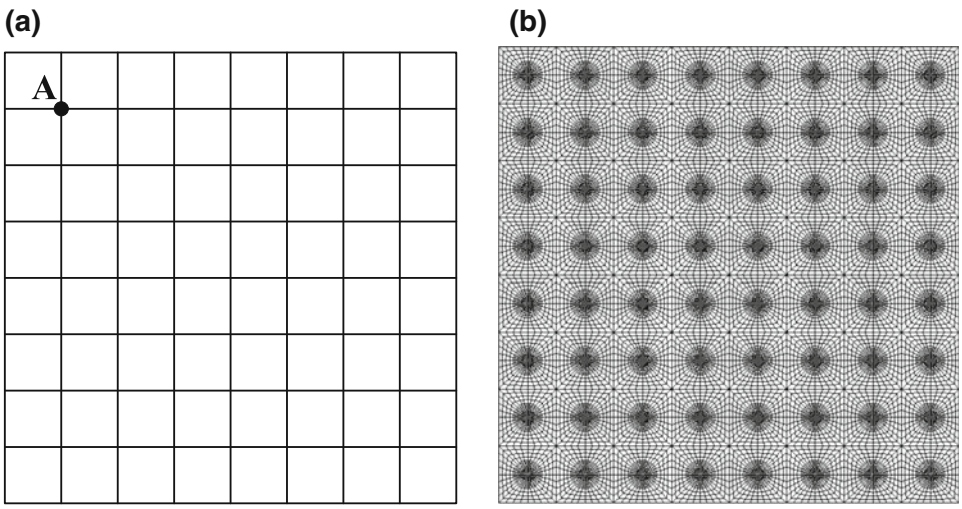

Fig. 22 Mesh discretization schemes for the EMsFEM and FEM-F: **a** coarse-scale grids; **b** fine-scale grids

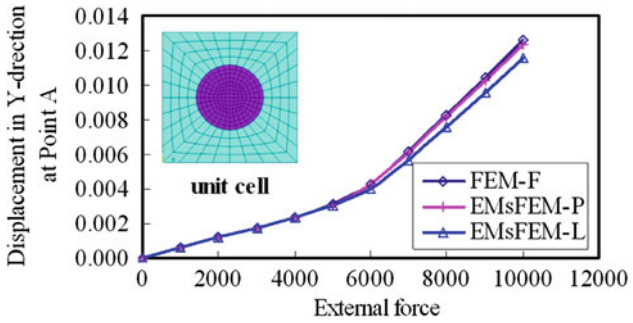

Fig. 23 Macroscopic load-displacement curves at Point A

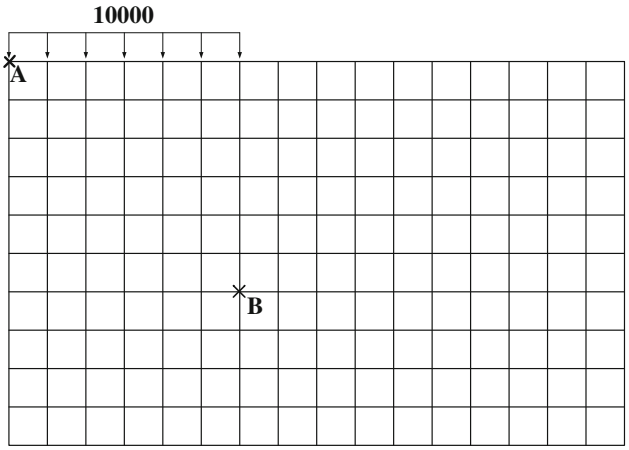

Fig. 26 Macroscopic FE model and its boundary conditions

stress $\sigma_Y^0 = 300$ and the unloading situation is considered to examine the feasibility of our method.

For simplicity, only the EMsFEM-P is considered in this example, and the results are compared with the FEM-F. The macroscopic load-displacement curves at Points A and B are plotted in Figs. 27 and 28, respectively. At the same time, the horizontal and vertical displacement fields of the overall structure obtained by the two methods at loading state P are shown in Figs. 29 and 30, respectively. As can be seen from the figures, the results obtained by the EMsFEM-P fit fairly

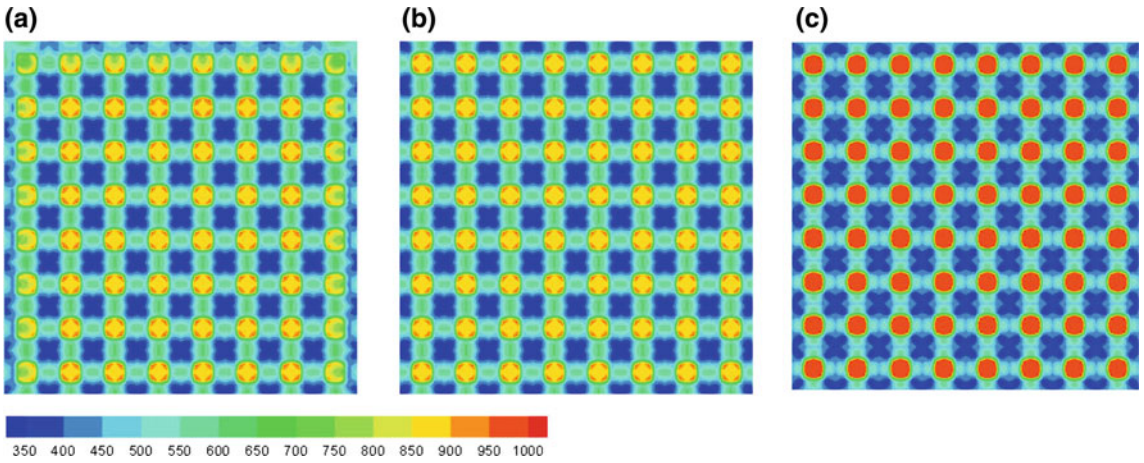

Fig. 24 Microscopic von-Mises stress at the final loading step: **a** FEM-F; **b** EMsFEM-P; **c** EMsFEM-L

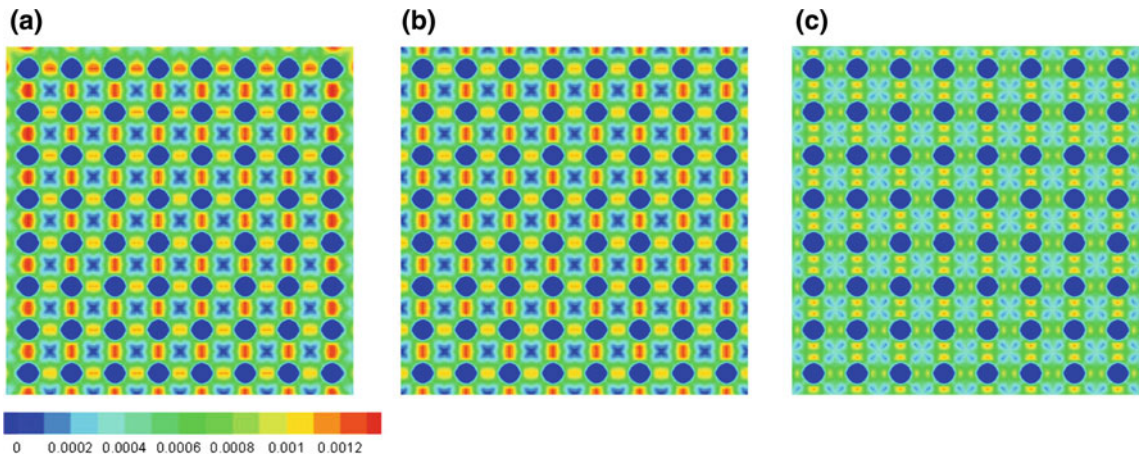

Fig. 25 Microscopic equivalent plastic strain at the final loading step: **a** FEM-F; **b** EMsFEM-P; **c** EMsFEM-L

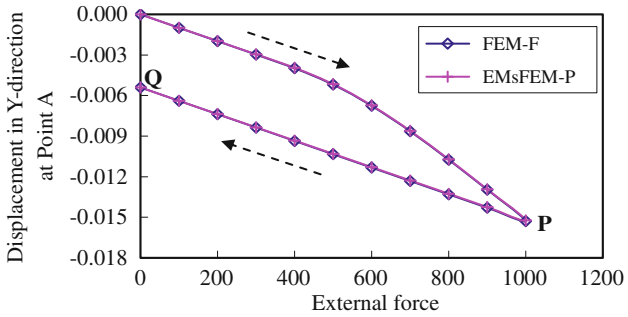

Fig. 27 Macroscopic load-displacement curves at Point A (The *dotted arrows* denote the loading and unloading direction)

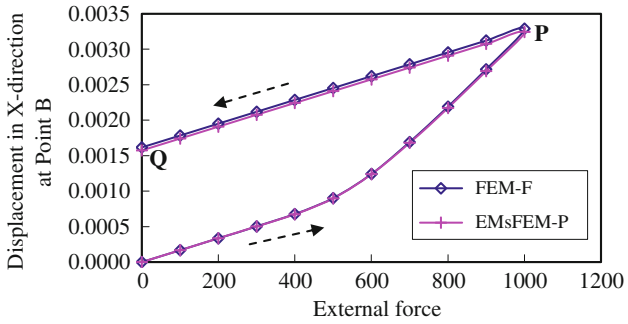

Fig. 28 Macroscopic load-displacement curves at Point B (The *dotted arrows* denote the loading and unloading direction)

well with the reference values for both loading and unloading situations. Figures 31 and 32 show the distributions of microscopic von-Mises stress at the state P and Q, respectively. We can see that the EMsFEM-P can capture well the evolution of microscopic variables along with the deformation histories.

Example 4 As mentioned before, our method can be easily used for computing the nonlinear problems with non-periodic microstructures (random microstructures are considered here), which is hard to be solved by the general homogenization methods. This is achieved by constructing the appropriate boundary conditions for the numerical base functions of each coarse element that can well capture the heterogeneities of fine-scale elements on the boundaries of sub-grids. In the EMsFEM, the generalized periodic boundary conditions can be used for this purpose. In this example, we consider a two-phase composite material beam model shown in Fig. 33. The size of the model is 240 × 48 and the size of the fine grid block is 1 × 1. The material property for each phase is the same as Example 1 and the macroscopic FE model and boundary conditions shown in Fig. 10 are used. The reinforcing phase (phase 2) is distributed in the fine grids randomly. Three cases are considered here, in which the volume fractions of the phase 2 are 10, 20 and 30%, respectively. At the same time, the initial yield stresses of phase 1 for the three cases are $\sigma_Y^0 = 170$, 140 and 100, respectively.

Figure 34 shows the macroscopic load-displacement curves at Point A for the three cases. As we can see that the results obtained by the EMsFEM-OP and reference values are in good agreement. The distributions of microscopic equivalent stress and equivalent plastic strain for the case 2 (volume fraction of the phase 2 is 20%) at the final loading step are plotted in Figs. 35 and 36, respectively, also a good agreement between the two methods can be found.

8 Computational cost comparison

The main purpose for developing multiscale methods is to solve some practical problems that are prohibitive by the traditional numerical methods (standard FEM, for example) due to the requisite of a tremendous amount of memory storage and CPU time. In this section, we make a rough estimate of the computer memory and CPU time in the EMsFEM, and compare them with those of the traditional FEM (FEM-F).

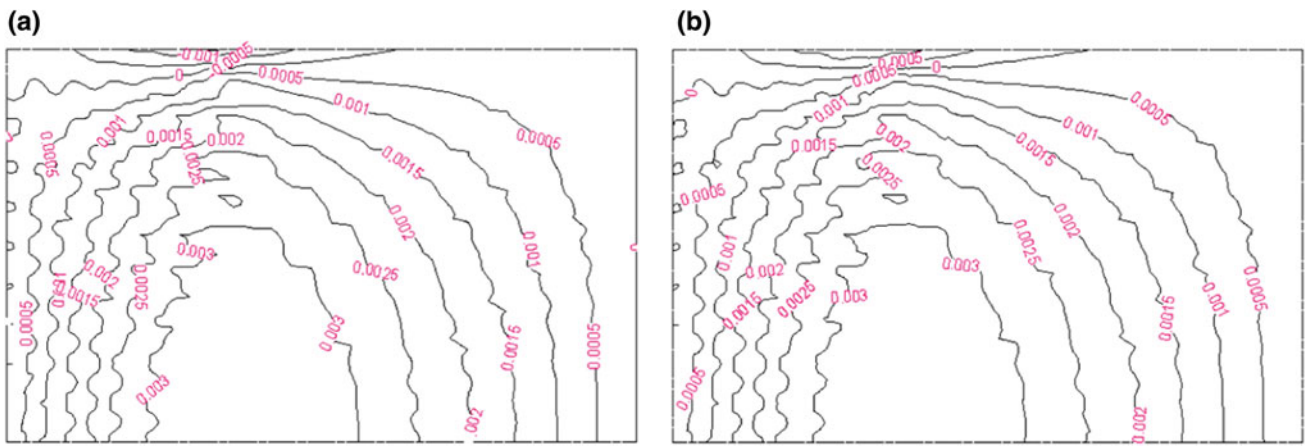

Fig. 29 The horizontal displacement field at state P: **a** FEM-F; **b** EMsFEM-P

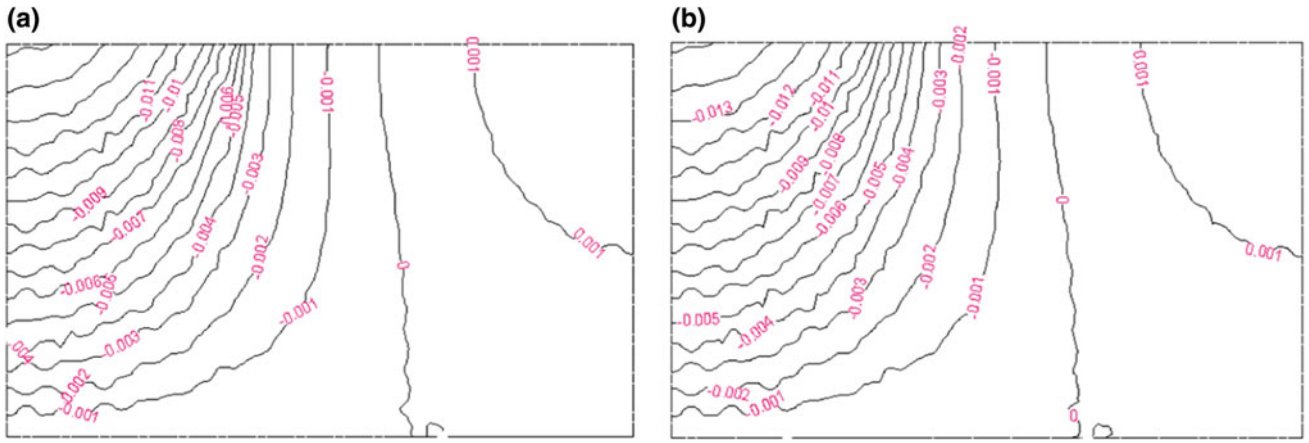

Fig. 30 The vertical displacement field at state P: **a** FEM-F; **b** EMsFEM-P

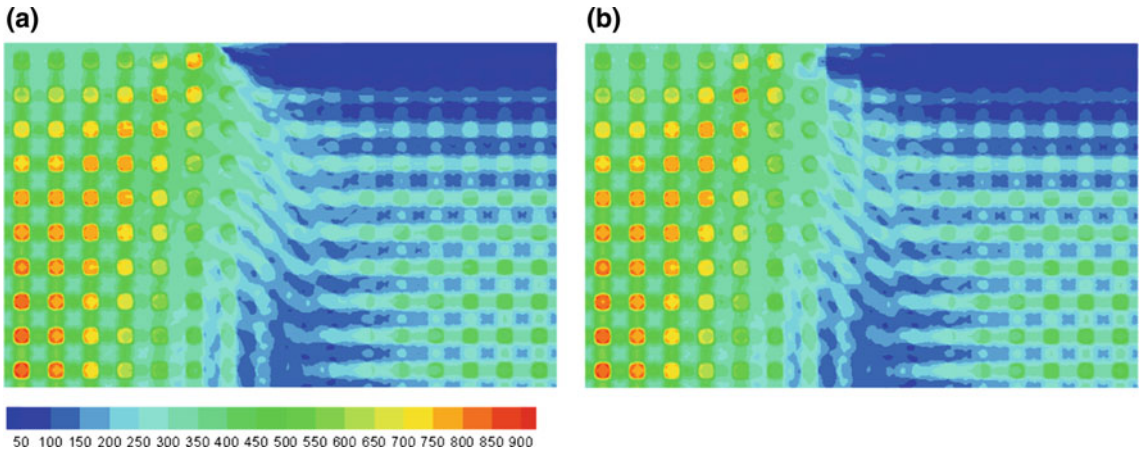

Fig. 31 Microscopic von-Mises stress at state P: **a** FEM-F; **b** EMsFEM-P

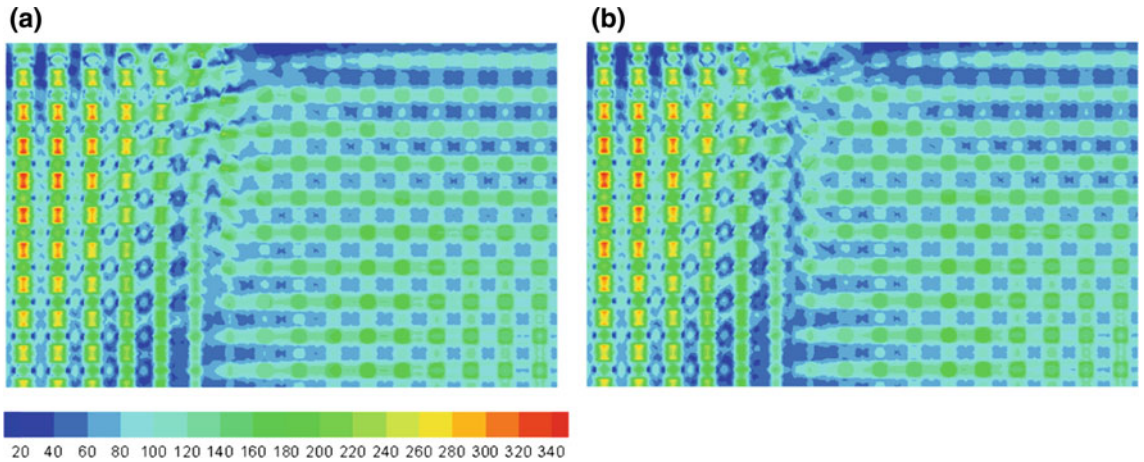

Fig. 32 Microscopic von-Mises stress at state Q: **a** FEM-F; **b** EMsFEM-P

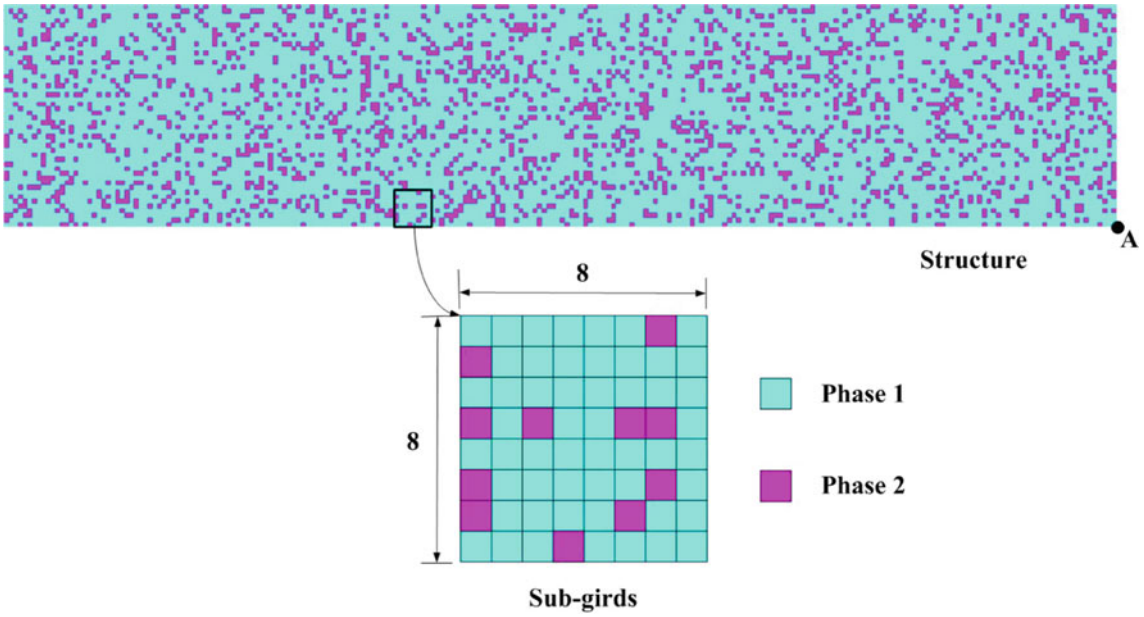

Fig. 33 Distribution of materials for composite material beam mode

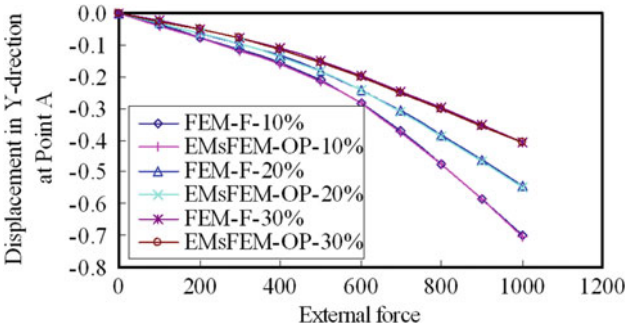

Fig. 34 Macroscopic load-displacement curves at Point A

Let's consider a numerical model with the number of coarse elements N and the number of fine elements within each coarse element M. Here the elements numbers are treated as an approximate representation of the nodes numbers for ease of description. Then for the FEM applied on the fine-scale model directly, the total number of elements at fine scale is $N \cdot M$ and the memory needed is $O(a \cdot N \cdot M)$, where a is the number of degrees of freedom on a single node. For the 2-D problems considered in the present paper, $a = 2$. For the EMsFEM applied on the coarse-scale models, if the serial computer is used, the memory needed is $O(a \cdot N) + N \cdot O(a \cdot M)$. In addition, if the oversampling technique is adopted in the EMsFEM, i.e., replace M by M' in the above expression, where M' is the number of fine grid elements within the oversampling region, the memory needed increases a little. It can be seen that the EMsFEM can offer a big saving in computer memory for large-scale

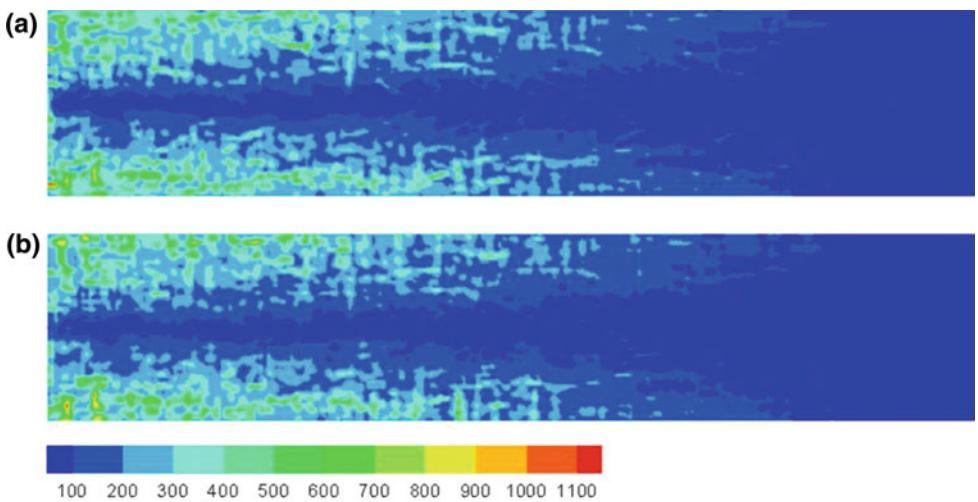

Fig. 35 Microscopic von-Mises stress for the case 2 at the final loading step: **a** FEM-F; **b** EMsFEM-OP

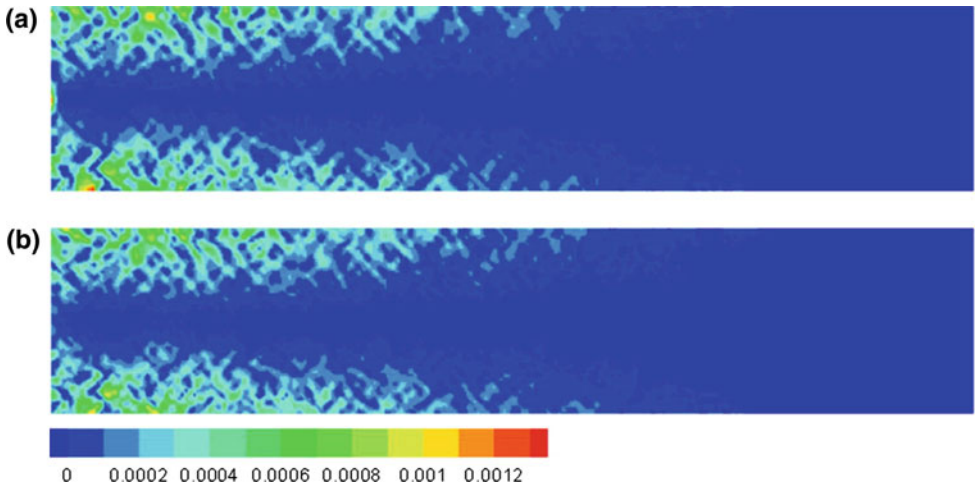

Fig. 36 Microscopic equivalent plastic strain for the case 2 at the final loading step: **a** FEM-F; **b** EMsFEM-OP

computation. For Example 3 in Sect. 7, $N = 160$, $M = 320$ and $N \cdot M = 51,200$. In this case, the FEM-F needs about 150 times more memory than the EMsFEM.

For the nonlinear problems, the operation count is $s_1 \cdot O(a \cdot N \cdot M)$ for the FEM-F, where s_1 is the total number of the iterative steps. The operation count for the EMsFEM consists of two parts, i.e., the preprocessing computation part and the nonlinear iteration computation part. In the preprocessing computation part, sub-grids problems need to be solved 6 times in each coarse element to obtain the base functions (i.e., $\mathbf{N}_i^x$ and $\mathbf{N}_i^y$, $i = 1, 2, 3$ need to be solved on subgrids problems, while $\mathbf{N}_4^x$ and $\mathbf{N}_4^y$ can be computed from Eq. 17). Thus, the operation count is $6 \cdot N \cdot O(a \cdot M)$ for the preprocessing part. Note that if the structures with periodic microstructures are considered, the base functions only be constructed on one coarse element (unit cell) and used for other ones, thus the preprocessing times can be omitted in this case. For the nonlinear iteration computation part, from the flow chart (Fig. 9) we can see that the operation count is about $s_2 \cdot (N \cdot O(a \cdot M) + O(a \cdot N))$, where s_2 is the total number of the iterative steps for the EMsFEM. Thus the total operation count is $6 \cdot N \cdot O(a \cdot M) + s_2 \cdot (N \cdot O(a \cdot M) + O(a \cdot N))$. Note that both of the FEM-F and the EMsFEM use the initial stiffness iteration procedure for the nonlinear analysis, the total number of the iterative steps are almost the same for the two methods. It should be mentioned that it is quite difficult to compare fairly the CPU times between the EMsFEM and FEM-F due to many factors (such as algorithm, hard ware, practical problems, etc), so the function expression of the operator 'O' is hard to define. But we can roughly estimate that it is the power of degrees of freedom if the serial computer is used. Thus, it also can be seen that the computing time is reduced significantly in our method when the structures are large. For Example 3, when the algorithms are implemented on the same computer, the FEM spends about 11150 seconds for all the loading and unloading process, while the EMsFEM only spends about 510 seconds.

It should be remarked here that, since the microscopic sub-girds problems in the EMsFEM are solved in each coarse element independently, our method can be easily developed for the parallel computing. In this context, the computational cost will be further reduced.

9 Conclusions

A new multiscale computational method for the elasto-plastic analysis of heterogeneous materials is proposed based on the idea of the extended multiscale finite element method (EMsFEM), in which the multiscale base functions are constructed numerically and employed to establish the relationship between the macroscopic displacement and microscopic stress and strain. By this means, the microscopic sub-girds (or RVEs) problems are solved on the coarse-scale element level rather than on the integration point level that are commonly used by many homogenization methods. This brings us a more convenient way to get directly the mechanical response on micro scale of the heterogeneous materials, which is important for strength prediction and nonlinear analyses. Extensive numerical examples for problems with both periodic and random microstructures are carried out and the results are compared with those of the direct FEM, it is shown that the multiscale method developed provides excellent prediction of the nonlinear response for the heterogeneous materials, especially under the (generalized) periodic boundary conditions. Moreover, the current method can reduce the memory storage and CPU time drastically for large scale structures.

Note that in our method the construction of the base functions and the downscaling computation for each coarse element are performed independently, thus, the current method can be easily developed for parallel computing. So the method developed has great potential for the nonlinear

analysis and dynamic analysis of large-scale problems that are intractable by the traditional numerical methods.

Acknowledgments The supports of the National Natural Science Foundation (11072051, 10721062, 90715037, 10728205, 51021140004), the 111 Project (B08014) and the National Key Basic Research Special Foundation of China (2010CB832704) are gratefully acknowledged.

References

1. Kanoute P, Boso DP, Chaboche JL, Schrefler BA (2009) Multiscale methods for composites: a review. Arch Comput Method Eng 16:31–75
2. Eshelby JD (1957) The determination of the elastic field of an ellipsoidal inclusion and related field. Proc Royal Soc Lond Ser A 241:376–396
3. Hashin Z, Strikman S (1963) A variational approach to the theory of the elastic behavior of multiphase materials. J Mech Phys Solids 11:127–140
4. Mori T, Tanaka K (1973) Average stress in the matrix and average elastic energy of materials with misfitting inclusions. Acta Metall 21:571–574
5. Hill R (1965) A self-consistent mechanics of composite materials. J Mech Phys Solids 13:213–222
6. Christensen RM, Lo KM (1979) Solutions for effective shear properties in three phase sphere and cylinder models. J Mech Phys Solids 27:315–330
7. Hori M, Nemat-Nasser S (1993) Double inclusion model and overall moduli of multiphase composites. Mech Mater 14:189–206
8. Dvorak G, Zhang J (2001) Transformation field analysis of damage evolution in composite materials. J Mech Phys Solids 49:2517–2541
9. Benssousan A, Lions JL, Papanicoulau G (1978) Asymptotic analysis for periodic structures. North Holland, Amsterdam
10. Suquet PM (1985) Local and global aspects in the mathematical theory of plasticity. In: Sawczuk A, Bianchi G (eds) Plasticity today: modelling, methods and applications. Elsevier, London pp 279–310
11. Terada K, Kikuchi N (1995) Nonlinear homogenization method for practical applications. In: Ghosh S, Ostoja-Starzewski M (eds) Computational Methods in Micromechanics. AMSE AMD, vol 212, pp 1–16
12. Fish J, Shek K, Pandheeradi M, Shephard M (1997) Computational plasticity for composite structures based on mathematical homogenization: theory and practice. Comput Meth Appl Mech Eng 148:53–73
13. Terada K, Hori M, Kyoya T, Kikuchi N (2000) Simulation of the multi-scale convergence in computational homogenization approaches. Int J Solids Struct 37:2285–2311
14. Ghosh S, LeeK Moorthy S (1996) Two scale analysis of heterogeneous elastic-plastic materials with asymptotic homogenization and Vornoi cell finite element model. Comput Meth Appl Mech Eng 132:63–116
15. Zhang HW, Wang H, Chen BS, Xie ZQ (2008) Analysis of Cosserat materials with Voronoi cell finite element method and parametric variational principle. Comput Meth Appl Mech Eng 197:741–755
16. Terada K, Kikuchi N (2001) A class of general algorithms for multi-scale analyses of heterogeneous media. Comput Meth Appl Mech Eng 190:5427–5464
17. Matsui K, Terada K, Yuge K (2004) Two-scale finite element analysis of heterogeneous solids with periodic microstructures. Comput Struct 82:593–606
18. Feyel F, Chaboche JL (2000) FE^2 multiscale approach for modeling the elastoviscoplastic behaviour of long fibre SiC/Ti composite materials. Comput Meth Appl Mech Eng 183:309–330
19. Lee K, Moorthy S, Ghosh S (1999) Multiple scale computational model for damage in composite materials. Comput Meth Appl Mech Eng 172:175–201
20. Fish J, Yu O, Shek K (1999) Computational damage mechanics for composite materials based on mathematical homogenization. Int J Numer Methods Eng 45:1657–1679
21. Fish J, Nagai G (2002) Nonlocal dispersive model for wave propagation in heterogeneous media. Part 1: One dimensional case . Int J Numer Methods Eng 54:331– 346
22. Fish J, Nagai G (2002) Nonlocal dispersive model for wave propagation in heterogeneous media. Part 2: Multi-dimensional case. Int J Numer Methods Eng 54:347–363
23. Zhang HW, Zhang S, Bi JY, Schrefler BA (2007) Thermo-mechanical analysis of periodic multiphase materials by a multiscale asymptotic homogenization approach. Int J Numer Methods Eng 69:87–113
24. Ibrahimbegovic A, Markovic D (2003) Strong coupling methods in multi-phase and multi-scale modeling of inelastic behavior of heterogeneous structures. Comput Methods Appl Mech Eng 192:3089–3107
25. Ghosh S, Lee k, Raghavan (2001) A multi-level computational model for multi-scale damage analysis in composite and porous materials. Int J Solids Struct 38:2335–2385
26. Brasile S, Casciaro R, Formica G (2007) Multilevel approach for brick masonry walls-part I: a numerical strategy for the nonlinear analysis. Comput Methods Appl Mech Eng 196:4934–4951
27. Babuska I, Osborn E (1983) Generalized finite element methods: Their performance and their relation to mixed methods. SIAM J Numer Anal 20:510–536
28. Babuska I, Caloz G, Osborn E (1994) Special finite element methods for a class of second order elliptic problems with rough coefficients. SIAM J Numer Anal 31:945–981
29. Hou TY, Wu XH (1997) A multiscale finite element method for elliptic problems in composite materials and porous media. J Comput Phys 134:169–189
30. Hou TY, Wu XH, Cai ZQ (1999) Convergence of a multiscale finite element method for elliptic problems with rapidly oscillating coefficients. Math Comput 68:913–943
31. Chen ZM, Hou TY (2003) A mixed multiscale finite element method for elliptic problems with oscillating coefficients. Math Comput 72:541–576
32. Efendiev Y, Ginting V, Hou TY, Ewing R (2006) Accurate multiscale finite element methods for two-phase flow simulations. J Comput Phys 220:155–174
33. Aarnes JE (2004) On the use of a mixed multiscale finite element method for greater flexibility and increased speed or improved accuracy in reservoir simulation. Multiscale Model Sim 2:421–439
34. Aarnes JE, Krogstad S, Lie KA (2006) A hierarchical multiscale method for two-phase flow based upon mixed finite elements and nonuniform coarse grids. Multiscale Model Sim 5:337–363
35. Efendiev Y, Hou TY, Ginting V (2004) Multiscale finite element methods for nonlinear problems and their applications. Commun Math Sci 2:553–589
36. Jenny P, Lee SH, Tchelepi HA (2003) Multi-scale finite volume method for elliptic problems in subsurface flow simulation. J Comput Phys 187:47–67
37. He X, Ren L (2005) Finite volume multiscale finite element method for solving the groundwater flow problems in heterogeneous porous media. Water Resour Res 41:W10417. doi:10.1029/2004WR003934
38. Zhang HW, Wu JK, Fu ZD (2010) Extended multiscale finite element method for mechanical analysis of periodic lattice truss materials. Int J Multiscale Comput 8:597–613

39. Zhang HW, Wu JK, Fu ZD (2010) Extended multiscale finite element method for elasto-plastic analysis of 2D periodic lattice truss materials. Comput Mech 45:623–635
40. Belytschko T, Liu WK, Moran B (2000) Nonlinear finite elements for continua and structures. John Wiley & Sons Ltd, San Francisco
41. Simo JC, Hughes TJR (1998) Computational Inelasticity. Springer, Berlin